Deeply Virtual Electroproduction of Mesons and Photons with JLab at 12 GeV

V.D. Burkert, B. A. Mecking, E.S. Smith
Jefferson Lab, Newport News, VA 23606

L. Elouadrhiri, S. Stepanyan
Christopher Newport University, Newport-News, VA 23606
& Jefferson Lab, Newport News, VA 23606

C. Hyde-Wright, A. Radyushkin
Old Dominion University, Norfolk, VA 23529
& Jefferson Lab, Newport News, VA 23606

J.P. Didelez, M. Guidal, C. Hadjidakis, E. Hourany
Institut de Physique Nucléaire, Orsay, France F-91406

F. Klein
Florida International University, Miami, FA 33199
& Jefferson Lab, Newport News, VA 23606

M. Garcon, P. Guichon, J.M. Laget, F. Sabatie
CEA/Saclay, DAPNIA/SPhn, Gif-sur-Yvette Cedex, France F-91191

M. Battaglieri, R. De Vita, M. Ripani, M. Taiuti
INFN, Genova, Italy

P. Stoler
Rensselaer Polytechnic Institute, Troy, NY 12180

M. Vanderhaeghen
University of Mainz, Mainz, Germany D-55099

R. Minehart, C. Smith
University of Virginia, Charlottesville, VA 22901

1 Introduction

Much of the internal structure of the nucleon has been revealed during the past three decades through the inclusive scattering of high-energy leptons on the nucleon in the Bjorken -or "Deep Inelastic Scattering" (DIS)- regime ($Q^2, \nu \gg$ and $x_B = \frac{Q^2}{2M\nu}$ finite). Simple theoretical interpretations of the experimental results and quantitative conclusions can be reached in the framework of the parton model and QCD when one sums over all possible hadronic final states. For instance, *unpolarized* DIS led to the discovery of the quark and gluon substructure of the nucleon, with the quarks carrying about half of the nucleon momentum. Furthermore, *polarized* DIS revealed that about 25% of the spin of the nucleon is carried by the quarks' intrinsic spin. Now, with the advent of the new generation of high-energy, high-luminosity lepton accelerators, combined with large-acceptance spectrometers, a wide variety of exclusive processes in the Bjorken regime can be envisioned to become accessible experimentally. Until recently, very few exclusive processes could be treated in the framework of pQCD and compared to experimental data (typical examples are the $\pi^0\gamma\gamma^*$ transition form factor and the elastic form factors of the pion and the nucleon). Fundamental information on the structure of the nucleon has been obtained from such analyses, from the shape of light-cone meson wave functions (or distribution amplitudes) to the scale of the intrinsic transverse momentum of the partons in the nucleon (or Fermi motion), Sudakov effects, etc.

The recently developed formalism of "Generalized Parton Distributions" (GPDs) (also called "Off-Forward Parton Distributions" [1, 2] -OFPDs- or "Skewed Parton Distributions" -SPDs-) - allows us to enlarge these types of exclusive processes and analyses to the broad class of processes which are the electroproduction of mesons and photons on the nucleon. For the first time the GPDs provide a unifying picture between a entire set of fundamental quantities of hadronic structure such as: nucleon form factors which are related to the vector and axial vector currents, the polarized and unpolarized parton distributions, the spin content components of the nucleon which are due to orbital excitations.

The theoretical framework of GPD's is summarized in the attached paper by Anatoly Radyushkin [**?**].

From the phenomenological point of view, the extraction of the GPD's from data is not a simple matter; it requires an extensive experimental program, and detailed analyses with controlled theoretical corrections.

- The GPD's are defined for each quark flavor. This means that we need to carry out a "flavor" separation, requiring measurement of different isospin channels (for example, ρ and ω or $\rho^\pm$ production are needed to separate u and d contributions).

- GPD's come in two forms, so-called "unpolarized" and "polarized". This separation can be carried out by measuring vector meson production and pseudo-scalar meson production, respectively.

- GPD's enter cross sections in the form of integrals. This means that a "deconvolution" procedure is needed and that measurements of cross sections alone are not sufficient. It is also important to measure spin observables, which involve direct measurement of GPD's at a specific kinematical point. The combination of these observables, which appear with different weights and in different channels should be sufficient to uniquely constrain the GPD's.

The complete extraction of the GPD's presents an extensive program, not a single experiment, involving the measurement of a variety of channels and observables. A global analysis will be required to definitively determine the GPD's from a large set of measurements.

In this framework we propose to investigate in a systematic fashion, the following exclusive meson and photon electroproduction reactions, up to the highest possible Q^2.

- $eN \to e'N\gamma$
- $eN \to e'N(\rho^{\pm}, \omega)$
- $eN \to e'N(\pi^{\pm,0}, \eta)$

Our goal is to simultaneously measure the Q^2, x_B and t dependences of cross sections, beam asymmetries (for DVCS) and transverse polarized target asymmetries (for meson production). These observables involve the leading order pQCD amplitudes, which are directly comparable to the GPD's formalism. Toward this end, a large acceptance spectrometer is highly desirable, as it will allow mappping the varies dependences for all channels, simultaneously.

GPD's may be explored in a wide range of kinematics: $\approx$.001< x_B <.9, Q^2 >2 GeV^2 and -t<1.5 GeV^2. This program requires

- high energy to reach the required high Q^2 @ small x_B,
- high luminosity to compensate for the fast drop of exclusive cross sections with Q^2 and hadronic cms energy,
- good detector resolution to identify exclusive channels,
- large acceptances for charged particle and neutral particle detection to measure varies channels simultaneously, and over a large kinematics range, and to guarantee the exclusivity of the process.

JLab at 12 GeV. with the proposed CLAS detector upgrade will meet most of these requirements, although the beam energy of 11 GeV for electron scattering experiments will limit the kinematical range accessible.

The program presented here is the first one to explore in a systematic fashion this new GPD domain of hadronic physics. The field is currently in full expansion on the theoretical side. Other experimental facilities, such as COMPASS, HERMES, JLAB at 6 GeV are currently considering similar studies. They will provide some extremely useful pieces of information, such as beam asymmetries for DVCS, transverse target spin asymmetries for mesons, exclusive cross sections at high Q^2, over a limited kinematical range.

in a very near future. However, it should be clear that, due to either luminosity (HERMES, COMPASS) or beam energy (JLab 6 GeV) limitations, a full program with, ultimately, a complete deconvoluton of the GPD's cannot be carried out with these existing facilities. (Also, in the case of COMPASS and HERMES, truly exclusive measurements are not possible at this time although there are plans for the installion of recoil detectors in the near future at these facilities. These will allow the necessary selection of exclusive processes. For instance, no facility can currently measure truly exclusive processes beyond $\approx$ 5 GeV^2, in any the x_B range, and especially in the valence quark region.

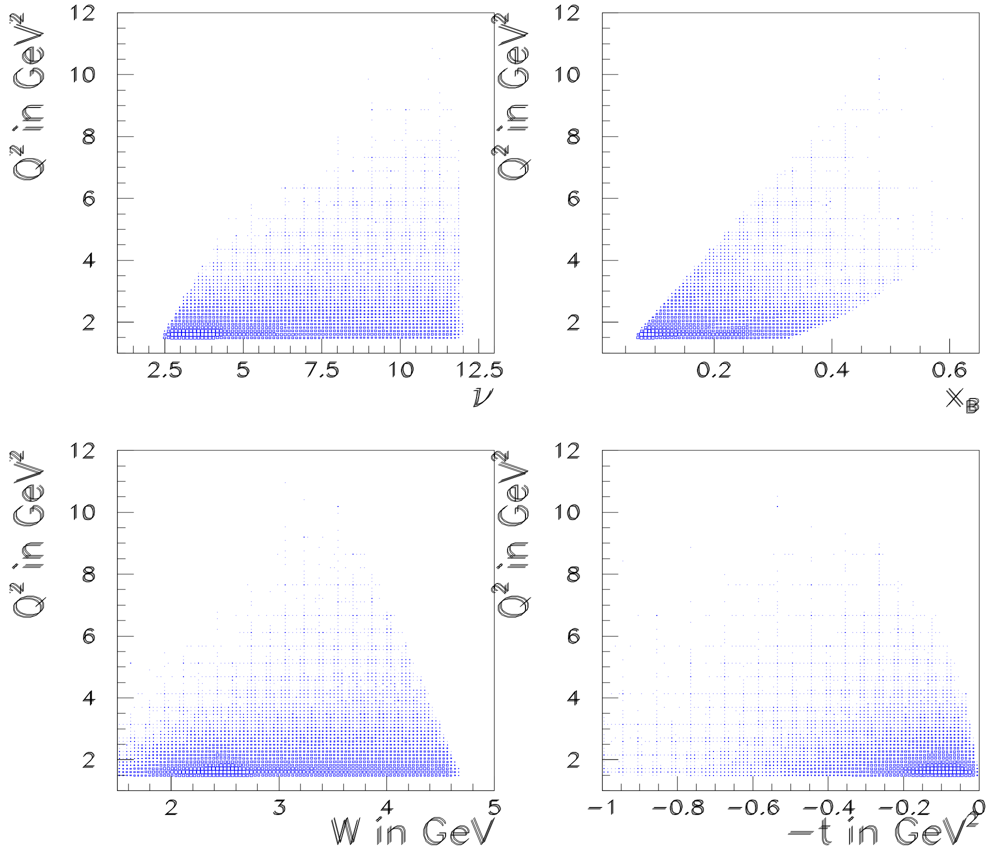

Figure 1: Correlation plots between Q^2, W, x_B and t. Domains accessible with a 12 GeV beam. In all figures except the bottom left one, the cut W> 2 GeV has been imposed.

Let us note a this stage that the $ep \to e'(\rho,\omega)p$ process is already the subject of an approved exploratory experiment at Jlab (E99-105 [3], approved at PAC 16 for Hall B, with a 6 GeV beam. A Deep Virtual Compton Scattering experiment is being presented at PAC 18 for Hall A [4].

The proposal is organized as follows. After a brief review of the GPD formalism, we present feasibility studies for 3 main processes with the CLAS detector, i.e. $ep \to e'\rho p$, $ep \to e'\pi^+ n$ and $ep \to e'\gamma p$ including kinematical domains attainable, count rates estimates, and observables to measure. Also, we review the existing data for each channel.

For meson production channels, it will be necessary to separate the longitudinal parts of the cross sections to make direct connection with the GPD formalism which relies on the factorization of the longitudinal part. We will present what we expect to achieve with the Rosenbluth technique for the π^+ channel and the study of the decay angular distribution for the ρ channel.

2 Phenomenology of the GPDs

We briefly review in this section the formalism of the Generalized Parton Distributions. GPDs parameterize the structure of the nucleon in leading-order pQCD. In recent years, Ji [1] and Radyushkin [2] have shown that the leading-order pQCD deeply virtual Compton scattering (DVCS) amplitude in the forward direction can be factorized into a hard-scattering part (exactly calculable in pQCD), and a non-perturbative nucleon structure part as illustrated in Fig. 2a. In these so-called "handbag" diagrams, the lower blob represents the structure of the nucleon and can be parameterized, at leading-order pQCD, in terms of four structure functions, known as the GPDs.

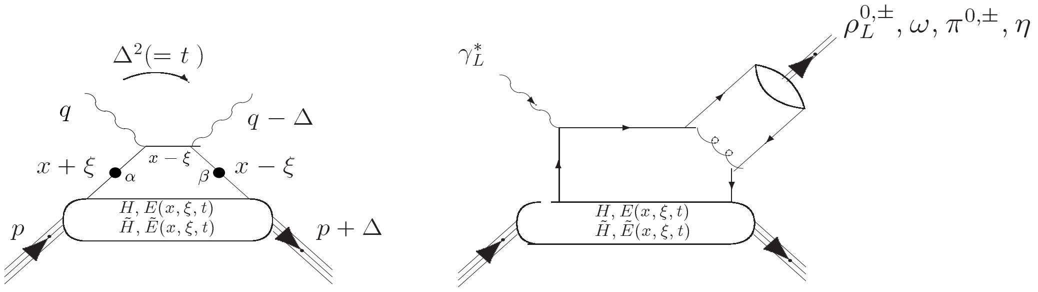

Figure 2: "Handbag" diagrams for (a) DVCS (left) and (b) meson production (right).

The GPDs are defined as $H, \tilde{H}, E$, and $\tilde{E}$, and depend upon three kinematic variables: x, ξ, and t. x is the momentum fraction of the struck quark in the quark loop and, as such, is not directly accessible experimentally. ξ is the longitudinal-momentum fraction of the transfer Δ with $\xi = x_B/(2 - x_B)$. $t = \Delta^2$ is the standard momentum transfer between the final-state meson and the virtual photon.

H and E are spin-independent and $\tilde{H}$ and $\tilde{E}$ are spin-dependent functions. More precisely, the light-cone matrix element of the bilocal quark operator that enters in these hard-electroproduction reactions (represented by the lower blobs in Fig. 2) is at leading twist in Q^2 given by:

$$
\begin{aligned}
&\frac{P^+}{2\pi} \int dy^- e^{ixP^+y^-} \langle p^{'}|\bar{\Psi}_\beta(-\frac{y}{2})\Psi_\alpha(\frac{y}{2})|p\rangle\Bigg|_{y^+=\vec{y}_\perp=0} \\
&= \frac{1}{4}\Bigg\{(\gamma^-)_{\alpha\beta}\left[H^q(x,\xi,t)\ \bar{N}(p^{'})\gamma^+ N(p)\ +\ E^q(x,\xi,t)\ \bar{N}(p^{'}) i\sigma^{+\kappa}\frac{\Delta_\kappa}{2M_N}N(p)\right] \\
&\quad +(\gamma_5\gamma^-)_{\alpha\beta}\left[\tilde{H}^q(x,\xi,t)\ \bar{N}(p^{'})\gamma^+\gamma_5 N(p)\ +\ \tilde{E}^q(x,\xi,t)\ \bar{N}(p^{'})\gamma_5\frac{\Delta^+}{2M_N}N(p)\right]\Bigg\}\ . \quad (1)
\end{aligned}
$$

This formula explicitly shows the vector (axial) nature of the H, E ($\tilde{H}$, $\tilde{E}$) GPDs associated or not with the γ_5 matrix.

The GPDs H and $\tilde{H}$ are generalizations of the parton distributions measured in deep inelastic scattering. In the forward direction (defined by $q = q'$), H reduces to the quark distribution $q(x)$ and $\tilde{H}$ to the quark-helicity distribution $\Delta q(x)$ measured in deep inelastic scattering. Furthermore, at finite momentum transfer, there are model-independent sum rules that relate the first moments of these GPDs to the standard elastic form factors. Also Ji [1] has shown that the second moment of these GPDs gives access to the sum of the quark spin and the quark orbital angular momentum to the nucleon spin, which may shed light on the "spin-puzzle". The GPDs reflect the structure of the nucleon independently of the reaction that probes the nucleon. They can also be accessed through the hard exclusive electroproduction of mesons -$\pi^{0,\pm}$, $\rho^{0,\pm}$, ω, ϕ,...- (see Fig. 2b) for which a QCD factorization proof was given recently [5]. In this proof it was shown that factorization applies when the virtual photon is longitudinally polarized because, in this case, the end-point contributions to the meson wave function are power suppressed. It was also shown that the cross section for a transversely polarized photon is suppressed by $1/Q^2$ compared to a longitudinally polarized photon, so that asymptotically, only σ_L survives. Ref. [5] showed as well that leading-order pQCD predicts that the vector meson channels ($\rho_L^{0,\pm}$, ω_L, ϕ_L) are sensitive only to the unpolarized GPDs (H and E), whereas the pseudoscalar channels ($\pi^{0,\pm}, \eta, ...$) are sensitive only to the polarized GPDs ($\tilde{H}$ and $\tilde{E}$). In comparison to meson electroproduction, we recall that DVCS depends on *both* the polarized and unpolarized GPDs. Therefore, by selecting specific mesons in the final state one selects the spin-dependent or spin-independent generalized parton distributions. Note that in this latter case, one can access polarized nucleon structure information without any polarization of external particles.

For a first exploratory approach, vector meson and charged pion channels hold the best promise due to the relatively high cross sections. First estimates for cross sections at forward angles were given in Refs. [6, 7] using an educated guess for the H and $\tilde{H}$ GPDs. This consists of a product of elastic form factors and quark distributions measured in DIS. In this "toy" model, E and $\tilde{E}$ are set to 0, as they enter with a kinematic factor proportional to the momentum transfer, as shown in eq(1). This ansatz satisfies the model-independent sum rules linking the GPDs to the nucleon form factors, and reduces to the quark distributions from DIS in the forward direction. In other words, the normalization is well determined. In Ref. [8], estimates using a more sophisticated ansatz for the GPDs, including ξ dependence, are given.

The GPD formalism is valid at small momentum transfers t and large Q^2. Fig. 3 shows the forward $\gamma_L^*+p \rightarrow M+p$ cross sections as a function of Q^2, and compares the leading-order predictions with the ξ-dependent ansatz for different mesons. The leading-order longitudinal cross section $d\sigma_L/dt$ for meson electroproduction shows a $1/Q^6$ behavior. This scaling behavior is analogous to the one observed in DIS, and is a prediction of pQCD at large Q^2.

One sees that the ρ_L^0 and ω_L channels, which are sensitive to the *unpolarized* GPDs, yield the largest cross sections. Then come the π^+ and π^0 channels, which are proportional to the *polarized* GPDs. The π^0 channel is about a factor of 5 below the pseudovector part ($\tilde{H}$) of the π^+ channel due to the different isospin structure of the corresponding GPDs. In the π^0 channel, the u- and d-quark polarized GPDs enter with the same sign, whereas in the π^+ channel, they enter with opposite signs. As the polarized GPDs are constructed here from the corresponding polarized-parton distributions, the fact that the polarized d-quark distribution is opposite in sign to the polarized u-quark distribution, explains the difference of the predictions for the π^0 and π^+ channels.

It is important to measure the Q^2 dependence of the forward differential cross section at fixed x_B. It is still uncertain at which Q^2 value one will reach the scaling regime where the pQCD leading-order domain fully applies. It is expected to be between 5 and 10 GeV^2 which is attainable with a 12 GeV beam. In any case, the way the asymptotic $1/Q^6$ behavior is approached is an important source of information on pre-asymptotic effects. "Soft" contributions are expected to drop as $1/Q^8$. An estimate of these pre-asymptotic effects in hard electroproduction reactions in the valence region is given in Ref. [8], where the effects of the intrinsic transverse momentum dependence of the quarks in the nucleon and in the meson are quantified. We may also note that fully reaching the asymptotic regime is not necessary as long as the corrections can be controlled by perturbative QCD methods.

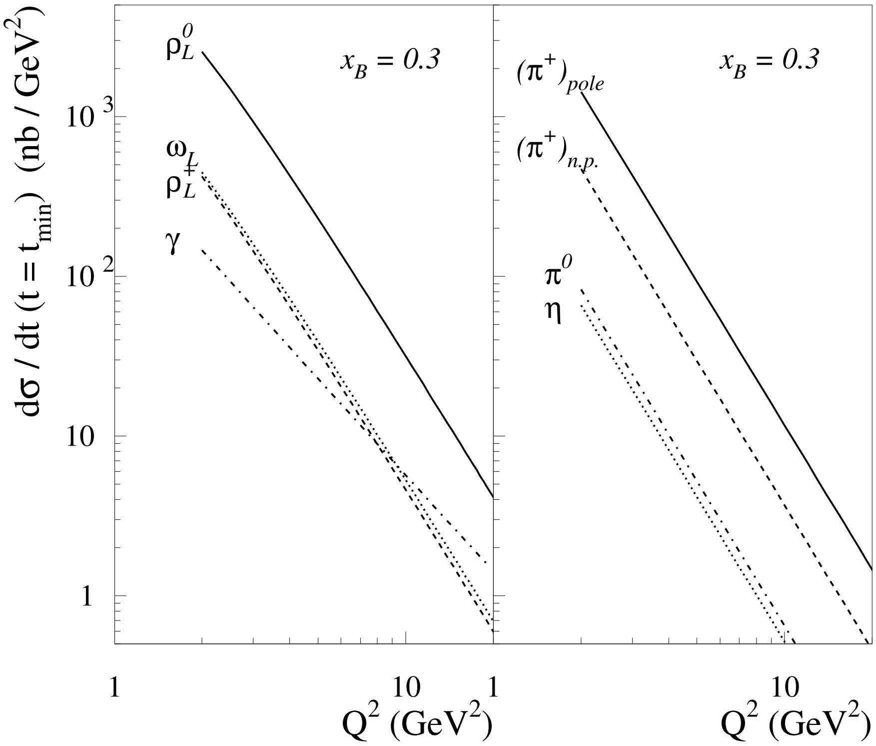

Figure 3: Scaling behavior of the leading-order predictions for the forward differential electroproduction cross section $d\sigma_L/dt$ on the proton for vector mesons (left panel) and pseudoscalar mesons (right panel). For the π^+-channel, the pion-pole contribution is given by the full line, whereas the pseudovector contribution is given by the dashed line. Also shown is the scaling behavior of the forward transverse cross section $d\sigma_T/dt$ for the leading-order DVCS cross section (dashed-dotted line in left panel).

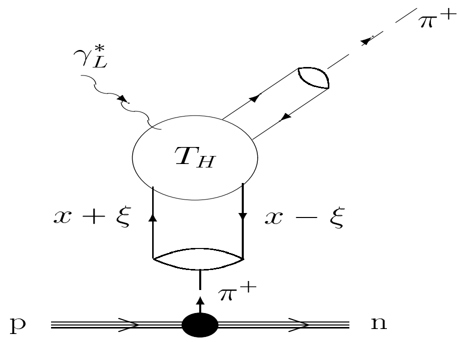

Figure 4: Pseudoscalar contribution to “hard” π^+ electroproduction. The virtual photon knocks out a pion from the meson cloud of the nucleon.

For the case of charged-pion electroproduction, it was shown recently in Refs. [9, 10] that there should be a strong contribution from the pseudoscalar structure (connected to $\tilde{E}$, see eq(1)) as it is related to the one-pion exchange process. Because of the small mass of the pion, this contribution should be quite important at forward angles. This feature is unique to the charged-pion process due to the proximity of the pion pole to the physical region. As explained in Ref. [9], one can picture the process in a simple way, where one identifies the pseudovector contribution (proportional to $\tilde{H}$) as the virtual photon interacting with a quark of the nucleon, which after a hard-gluon exchange, combines with a second quark of the nucleon to form the final pion (see Fig. 2b). The pseudoscalar contribution (proportional to $\tilde{E}$) represents the process where the virtual photon knocks out a pion from the meson cloud of the nucleon (see Fig. 4). These two processes are predicted to have distinctly different behavior in the x_B and t dependences of the cross sections. This deserves thorough experimental investigation.

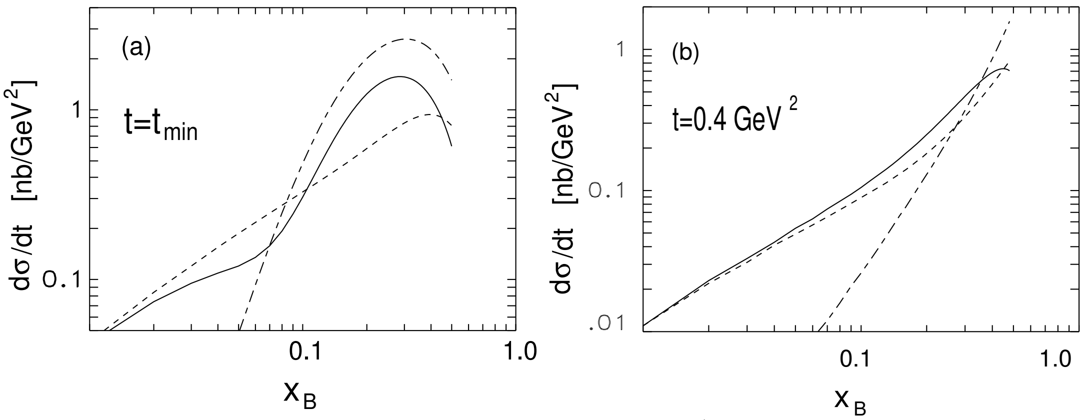

Figure 5: Differential production cross section for exclusive π^+ production through the scattering of longitudinally polarized photons from protons at $Q^2 = 10$ (GeV/c)^2 for (a) $t = t_{\rm min}$ and (b) $t = -0.4$ (GeV/c)^2. The dashed and dot-dashed curves show the pseudovector and pseudoscalar contributions, respectively.

It is seen in Fig. 3 that for π^+ electroproduction in the valence region ($x_B \approx$0.3) and in the forward direction, the pseudoscalar contribution (pion pole) is about three times as large as the pseudovector contribution. This was also found in the calculation of Ref. [9] that is shown in Fig. 5a for $t = t_{min}$. The authors of Ref. [9] concluded that one obtains a dominance of the pseudovector at $t = t_{min}$ only at quite small values of x_B. At larger momentum transfers, as shown in Fig. 5b for $-t$=0.4 (GeV/c)^2, the pseudoscalar contribution decreases faster. The pseudoscalar and the pseudovector contributions become comparable around $x_B \approx$0.2.

Finally, it will be very important to measure the π^+/π^0 ratio as no such pion pole "t-channel" exchange exists for π^0 production. Therefore, one should expect in the valence region (around x_B=.3) where the pion pole (i.e. the pseudo-scalar part) contributes for the π^+ channel and not for the π^0 channel, an enhancement of the π^+/π^0 ratio as shown on figure 6.

Clearly, detailed x_B (W) and t dependent experimental scanning is needed in order to validate and quantify these pictures for the π^+ channel.

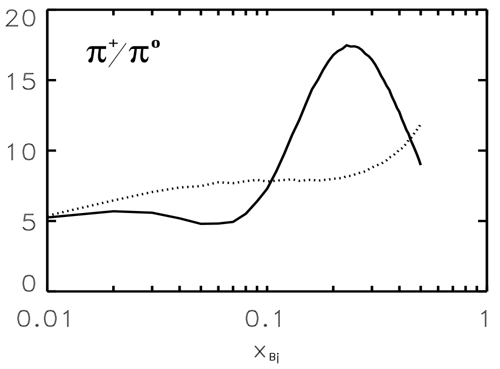

Figure 6: π^+/π^0 as a function of x_B. The contribution of the pion pole for the pi^+ channel which does not appear for π^0 production, produces an enhancement of this ratio in the valence region.

3 The $ep \to e'\rho p$ channel

3.1 Existing Data

Electroproduction of ρ mesons is the only exclusive process (together with the other vector meson channels, i.e. ω and ϕ) for which experimental data above the resonance region and at large Q^2 (i.e. $Q^2 > 4$ GeV^2) exist. At high C.M. energies (W), it is well known that the Perturbative Two Gluon Exchange Mechanism (PTGEM) dominates for Q^2 greater than a few GeV^2. This mechanism also implies a $\frac{1}{Q^6}$ behavior of σ_L [14] [15] (The PTGEM mechanism is illustrated on Fig.(9)). The PTGEM explains the fast increase of the cross section at high energy, which has also been confirmed by the more recent ZEUS data [16]. However, the PTGEM substantially underestimates the data at lower energies (around $W \approx$ 10 GeV). And this is the region where the quark exchange mechanism (QEM) of Fig.(7) is expected to contribute ($W < 10$ GeV corresponds roughly to x_B in the valence region at the high Q^2 values shown). The data shown in Fig.(8) strongly suggest that the deviation from the PTGEM of the data at lower energies can be attributed to the onset of the QEM. Furthermore, recent data from HERMES [17] in the W region 4 - 6 GeV and for Q^2 values up to 4 GeV^2 provide further evidence for the quark exchange mechanism. Going down in energy (but staying above the resonance region), the sensitivity to the QEM and consequently to the Generalized Quark Distributions increases. Fig. 7 shows the region accessible at JLab, i.e. the valence region ($x_B \simeq 0.3$) where the QEM is maximal.

In Fig.8, we have shown that existing data at intermediate W values (around $W \approx 10$ GeV) already suggest quark exchange mechanism at large Q^2. At the low Q^2 side, several data for exclusive electroproduction of vector mesons have been taken [18][19].

In Ref.[18], DESY data for exclusive ρ^0 electroproduction are shown in the W region 1.3 - 2.8 GeV and in the Q^2 range 0.3 - 1.4 GeV^2. Data closest to our kinematical domain of concern near the low Q^2 side were obtained at Cornell [19], where the exclusive ρ^0, ω and ϕ electroproduction has been measured in the range $1.9 < W < 4$ GeV (above the resonance region) and $0.7 < Q^2 < 4$ GeV^2.

Fig.10 shows the total longitudinal ρ cross section versus Q^2 for the Cornell data. The longitudinal cross section was obtained from an exponential form for the forward differential cross section. For comparison, the prediction of the QEM in terms of the OFPD's is also shown for the average value of $W = 2.65$ GeV and is extrapolated to the lower Q^2 of the Cornell data. It is seen that the order of magnitude of this QEM prediction which was found

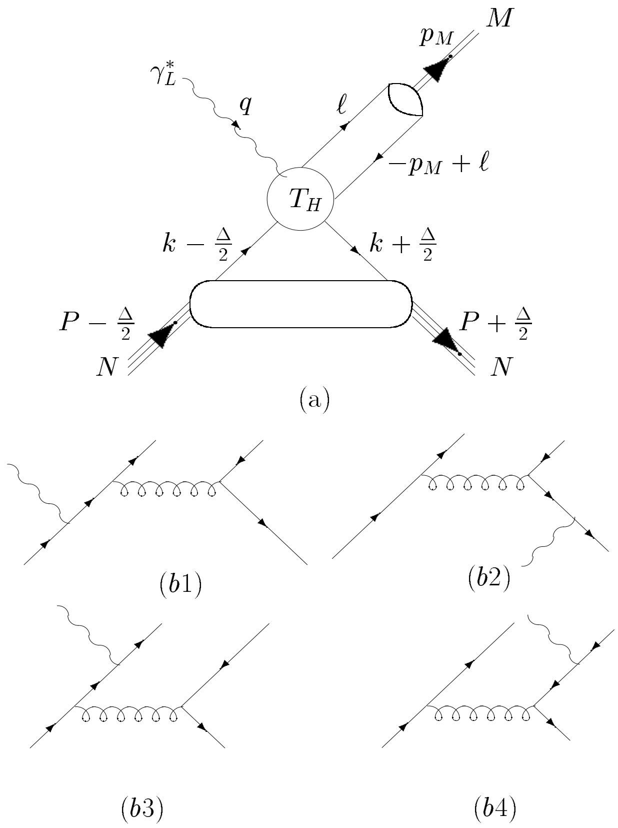

Figure 7: (a) Diagram for the factorized meson electroproduction amplitude. (c) Leading order diagrams for the hard scattering part T_H of the meson electroproduction amplitude.

on Fig.8 to be compatible with the data at higher Q^2, is also roughly in agreement with the Cornell data at lower Q^2. However, large Q^2 bins were used, which do not have the precision, nor a sufficiently large lever arm in Q^2 to test the Q^2 scaling behaviour of the leading order PQCD amplitude. Furthermore, the data shown in figure 10 mix different x_B values, which prevents any conclusion.

Obviously, much more precise data, in a larger Q^2 range, and at fixed x_B are needed to provide the information needed study to study the GPDs as proposed here.

The reaction $ep \to ep\omega$ has also been measured at Cornell in the same kinematical range as for the ρ. A diffractive production mechanism predicts a 1:9 ratio for $\sigma_\omega/\sigma_\rho$. The ω/ρ ratio for the Cornell data is shown in Fig.11. It is seen that in the range $2.8 < W < 3.7$ GeV, a ratio that is comparable to the one of a diffractive mechanism is found. However at lower W, a substantially higher ratio was found. At the photoproduction point this is understood as being due to the contribution of π^0 exchange to ω photoproduction, which dominates at lower W in comparison to the pomeron exchange mechanism at high W. It is only the latter one which gives a ratio of 1:9. Going to higher Q^2, this increased ω/ρ ratio in the region W = 2 - 3 GeV may be further evidence for the quark exchange mechanism. As shown in Fig.3, the QEM predicts a ω/ρ ratio of about 1:5 in the valence region, which is almost twice as much as expected in the diffractive domain. In the QEM this tatio is determined by the u and d-quark GPDs.

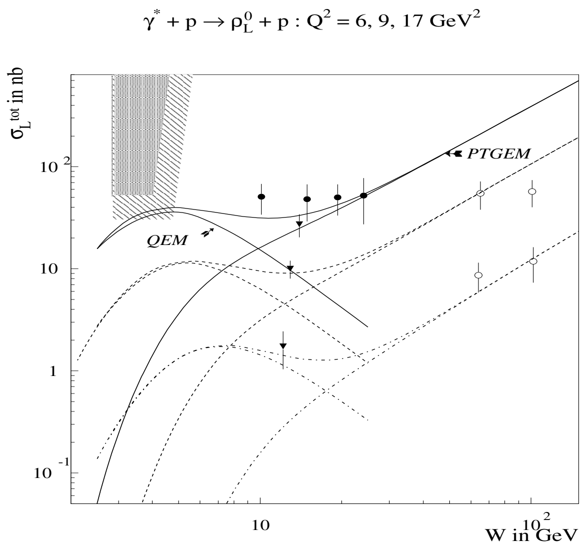

Figure 8: Total longitudinal cross section for ρ^0_L electroproduction as calculated in Ref.[6]. Data from NMC [11] (triangles) at $Q^2 = 5.5$ (highest point), 8.8 and 16.9 (lowest point) GeV^2, E665 [12] (black circles) at $Q^2 = 5.6$ GeV^2 and ZEUS [13] (open circles) at $Q^2 = 8.8$ (upper points) and 16.9 GeV^2 (lower points). Calculations are shown at $Q^2 = 6$ GeV^2 (full lines), $Q^2 = 9$ GeV^2 (dashed lines) and $Q^2 = 17$ GeV^2 (dashed-dotted lines). The curves which grow at high W correspond to gluon exchange whereas the curves which are peaked below W $\approx$ 10 GeV correspond to quark exchange. The incoherent sum of both mechanisms is also shown.
The two shaded areas on the top left part of the plot show the regions kinematically accessible at JLab with a 6 GeV and a 8 GeV electron beam (smaller and larger area respectively) NEEDS TO BE REDONE WITH 11 GEV.

3.2 Separation of longitudinal and transverse contributions

We recall that it is necessary at a first stage to identify the longitudinal part of the cross section for which the factorization theorem applies and the connection with the GPD formalism can be made. Longitudinal ρ^0_L's can be identified through the angular distribution of the vector meson decay. Assuming s-channel helicity conservation, or SCHC, the desired cross section : $\gamma^*_L p \to p(\rho^0_L, ...)$ can be extracted by analyzing the angular distribution. [1]

The angular distribution of the decay products of the ρ reflects its polarization state. Assuming the outgoing electron and proton are detected, measurement of only one decay pion is sufficient to determine the decay angular distribution. The decay pion defines an angle θ_{cm} which is the polar angle relative to the direction opposite to the recoiling target in the ρ center of mass frame (see figure 12). The $\cos(\theta_{cm})$ distribution follows the form :

$$W\left(\cos(\theta_{cm})\right) = \frac{3}{4}\left\{1 - r^{04}_{00} + (3r^{04}_{00} - 1)\cos^2\theta_{cm}\right\} \tag{2}$$

The matrix element r^{04}_{00} depends on Q^2 and W and is linked to the longitudinal polarization state of the ρ -for instance, r^{04}_{00}=1 (0) corresponds to pure longitudinal (transverse) polarization of the ρ respectively and, in terms of angular distribution, to $\frac{3}{2}\cos^2\theta_{cm}$

[1]The SCHC hypothesis can actually be tested by considering the interference response functions R_{TT} and R_{TL}, which are accessible with a large acceptance detector such as CLAS.

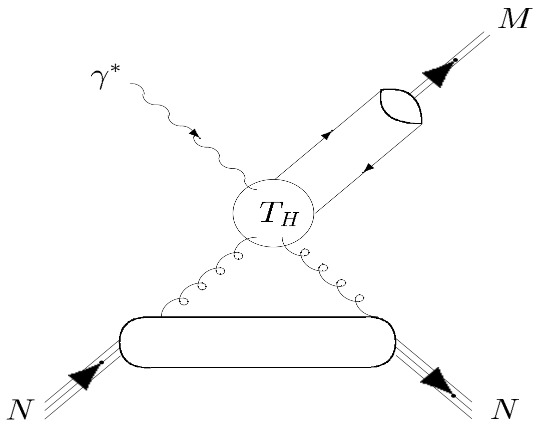

Figure 9: Perturbative 2-gluon exchange mechanism [14] [15].

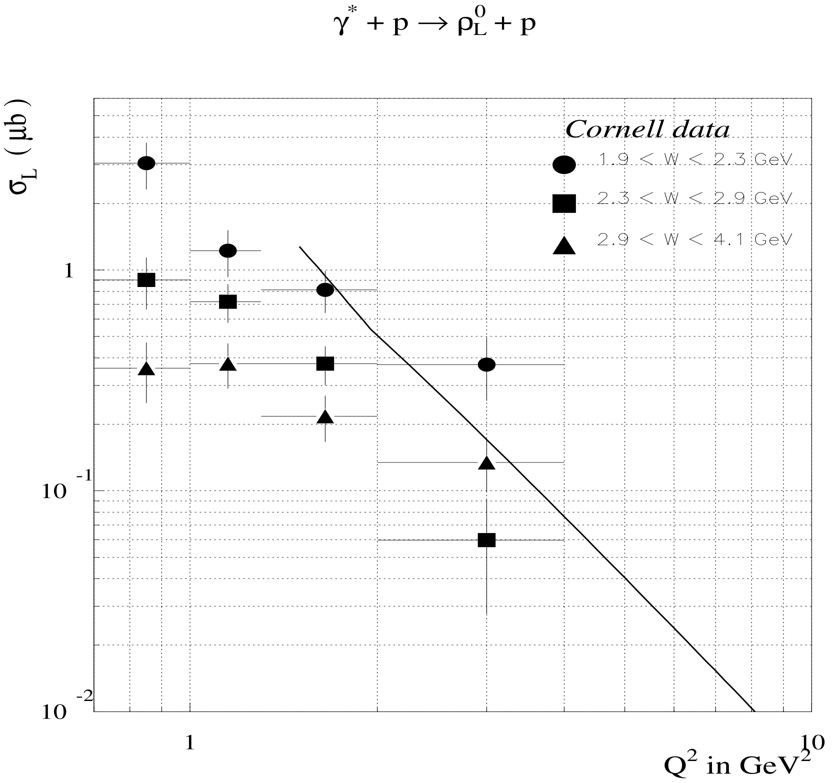

Figure 10: Longitudinal cross section data for exclusive ρ^0 electroproduction from Cornell [19] for W in the range 2 - 4 GeV and Q^2 values up to 3 GeV^2. The solid curve is the calculation for ρ^0_L electroproduction using the OFPD's at the average value $W = 2.65$ GeV of the Cornell data.

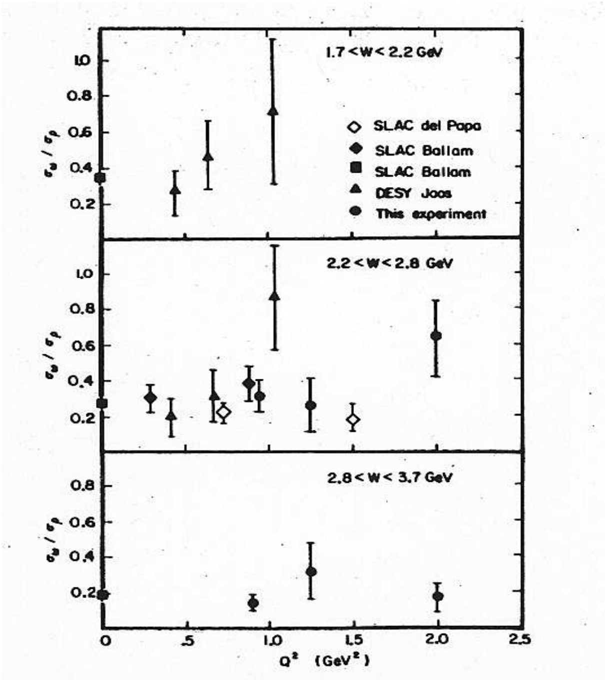

Figure 11: ω/ρ^0 ratio at different W as function of Q^2. The data are from Cornell [19].

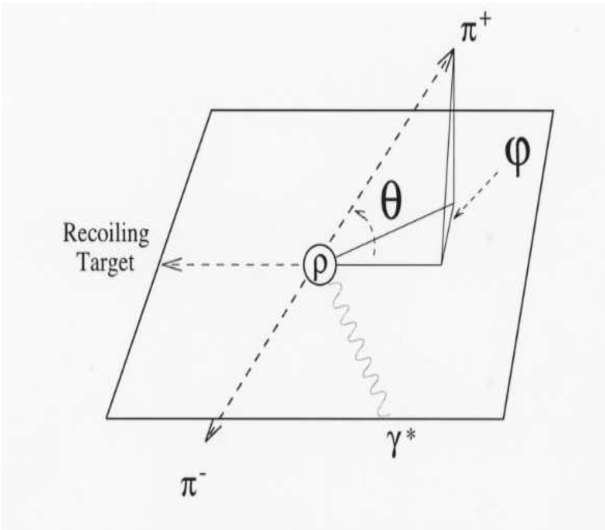

Figure 12: The polar angle θ_{cm} of the π^+ is defined, in the ρ rest frame, with respect to the z-axis antiparallel to the recoiling proton direction.

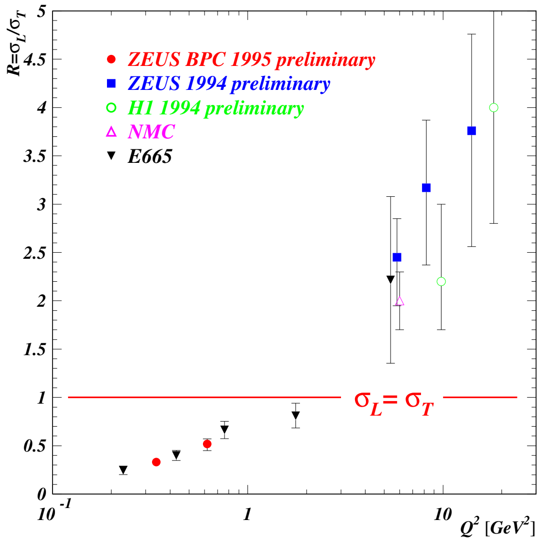

Figure 13: World data of $R = \frac{\sigma_L}{\sigma_T}$ as a function of Q^2 (assuming SCHC) [16].

($\frac{3}{4}\sin^2\theta_{cm}$) respectively-. Assuming s-channel helicity conservation (SCHC), one often links the ρ polarization to the virtual photon polarization and one defines :

$$R = \frac{\sigma_L}{\sigma_T} = \frac{1}{\epsilon}\frac{r^{04}_{00}}{1 - r^{04}_{00}} \tag{3}$$

The link is obvious : as r^{04}_{00} represents the longitudinal degree of polarization, $1 - r^{04}_{00}$ represents the transverse degree of polarization. One then divides by the degree of longitudinal polarization of the photons : ϵ.

R has been measured in many experiments. It is displayed in Figure 13 as a function of Q^2, though for a mixture of W values. The observed increase of R with Q^2 means that longitudinal ρ's are dominant at large Q^2. However, there are no data in the region of interest for this study at $Q^2 \approx 3$ GeV^2, and $2 < W < 3$ GeV, where it needs to be measured.

3.3 Simulation

To estimate the accuracy we will be able to achieve for a measurement of R, we generated events with the ratio R using the relationship :

$$R = \xi^2 \frac{Q^2}{M^2_\rho} \tag{4}$$

This formula is a results of the Vector Meson Dominance (VDM) approach [23], and describes the data of Figure 13 at intermediate Q^2 (≈ 3 GeV^2) with a value ξ^2= 0.3.

Figure 14 shows the simulated θ_{cm} angular distribution of the decay π^+ for different Q^2 bins. The CLAS acceptance has been taken into account in a parametric simulation. A luminosity of 10^{35} cm^{-2} s^{-1} was assumed, using a beam energy of 11 GeV, and a 400 hours run time. Bin size of 0.3< x_B <0.4, -0.2¡< $-t$ <0.4, ΔQ^2=1 GeV^2 have been assumed.

From the θ_{cm} distribution, one extracts the ratio R=$\frac{\sigma_T}{\sigma_L}$ as described above. Figure 15 shows the separated cross section for ρ electroproduction, with the purely statistical error bars.

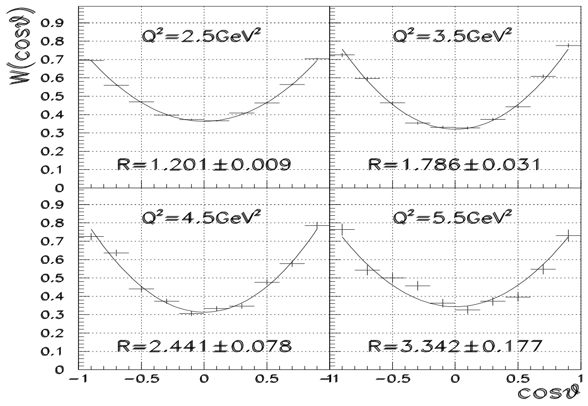

Figure 14: Simulated reconstruction of the θ_{cm} angular distribution of the decay π^+ in the ρ center of mass frame. Errors here are purely STATISTICAL. The result of the fit for the ratio R=$\frac{\sigma_T}{\sigma_L}$ is shown with the corresponding error. (.3< x_B <.4, -.2¡< $-t$ <.4, ΔQ^2=1 GeV^2), 400 hours of beam time, 10^35 cm^{-2} s^{-1}.

4 The $ep \to e'\pi^+n$ channel

The $ep \to e'\pi^+n$ reaction is the exclusive electroproduction reaction that is most easily accessible experimentally due to its relatively high cross section, and due to the simple identification of the exclusive reaction. It is therefore an ideal process to be studied over a large kinematical range, from the "soft" to "hard" domain.

As emphasized in the previous sections, the separation of the longitudinal response function of the reaction is essential to make the connection with the GPD formalism that relies on the factorization of the longitudinal part. Its study, as a function of Q^2 and x_B, is fundamental to test the validity of the pQCD predictions and their domain of applicability. The L/T separation for pions obviously cannot be accomplished like for vector mesons through the study of their decay angular distributions. The objective here is to rely on the Rosenbluth technique. In the following we show that we can do so up to $Q^2 \approx 6$ (GeV/c)^2.

L/T separated data for the electroproduction of π^+ on the nucleon above the resonance region and $Q^2 > 1$ (GeV/c)^2 is extremely scarce. The only measurement has been done by Bebek *et al.* [20] at the Cornell accelerator. In that experiment, five points were measured in total. Fig. 16 shows the data measured near $< x_B >= 0.3$ as a function of Q^2. The two large Q^2 points are not incompatible with the leading-order pQCD calculation [8]. The leading-order PQCD calculation is done here with a running coupling constant extrapolated to lower Q^2. Power corrections to the leading-order amplitude (pre-asymptotic effects such as intrinsic transverse momentum dependence and overlap contribution to the pion form factor for instance) are also expected to contribute in this Q^2 domain. Clearly, a precise measurement and scan of this Q^2 region is needed in order to draw firm conclusions regarding the domain of dominance and validity, and the nature of the various contributions.

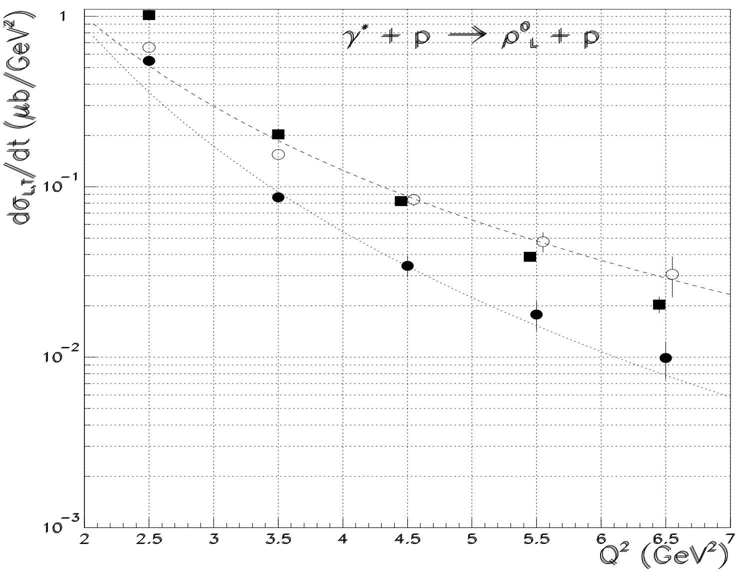

Figure 15: Simulation of the L/T separated cross section $d\sigma/dt$ for ρ electroproduction with a 11 GeV electron beam (same running conditions as in figure 14. Black squares are the total (unseparated) cross section ($\sigma_{tot} = \sigma_T + \epsilon$). Full circles are σ_T, decreasing like $1/\mathrm{Q}^8$ (dotted line). Empty circles are σ_L, decreasing like $1/\mathrm{Q}^6$ (dashed line).

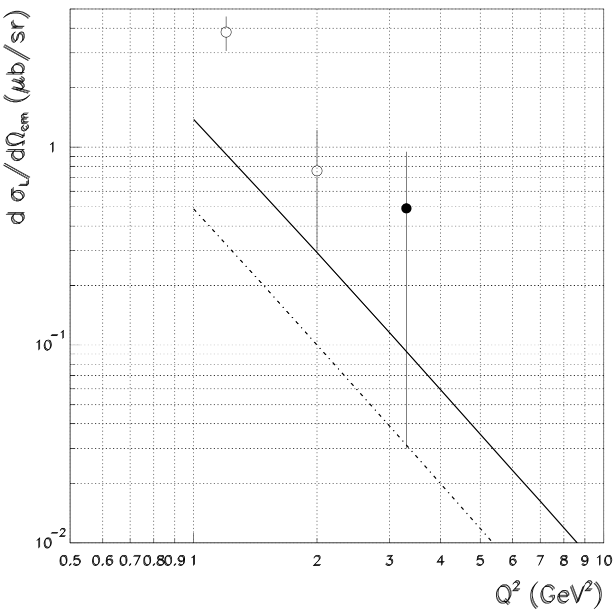

Figure 16: Longitudinal forward differential cross section for exclusive π^+ production as a function of Q^2 from the data of Bebek *et al.* [20]. Empty circles correspond to $< x_B >= 0.24$ and full circles to $< x_B >= 0.35$. The solid and dot-dashed curves are calculations of the total (pseudoscalar+pseudovector) and pseudoscalar contributions, respectively, for x_B=0.3 from Ref. [8]. The leading-order PQCD calculation was done here with a running coupling constant extrapolated to lower Q^2.

4.1 L/T separation using the Rosenbluth technique

In this section we demonstrate what should be feasible in CLAS for the L/T separation of the exclusive π^+ electroproduction using beam energies up to 11 GeV. The procedure to separate the longitudinal from the transverse cross section in electroproduction is well known. The general form of the unpolarized differential cross section for the reaction $ep \to e'\pi^+ n$ is:

$$\sigma_{\gamma^* p} = \sigma_T + \epsilon\sigma_L, \tag{5}$$

where σ_T, σ_L are the transverse and longitudinal cross sections, respectively, integrated over the out-of-plane angle ϕ. They depend on the variables Q^2 and W, and t the momentum tarnsfer between the virtual photon and the pion. ϵ represents the usual virtual photon polarization parameter.

In order to separate σ_T and σ_L, it is necessary to vary ϵ, which can only be done, keeping x_B and Q^2 fixed, by varying the beam energy (Rosenbluth separation). In the following, we will use 6, 8 and 11 GeV incident beams. For the identification of the reaction, it is sufficient to detect the scattered electron and the charged pion, the neutron being reconstructed by the missing-mass technique.

We present in Fig. 17 the results of the simulations for the Rosenbluth separation. We have used an event generator, adapted from Ref. [22], which scales as $\frac{1}{Q^6}$ for σ_L and $\frac{1}{Q^8}$ for σ_T. Events were generate assuming a luminosity of 10^{35} cm^{-2}s^{-1} and 1600 hours of 100% efficient beam time for both the 6 and 8 GeV beam energies. As an example, Fig. 17 shows the reconstructed cross section as a function of ϵ from the Monte Carlo for different Q^2 values at $< x_B >$=0.35 and $< -t >$=0.3 (GeV/c)^2. For the binning, we took Δx_B=0.1,

Δt=0.2 (GeV/c)^2 and ΔQ^2=0.2 (GeV/c)^2. The CLAS acceptance has been taken into account and a 4% error bars for systematics have been added quadratically to the statistical errors.

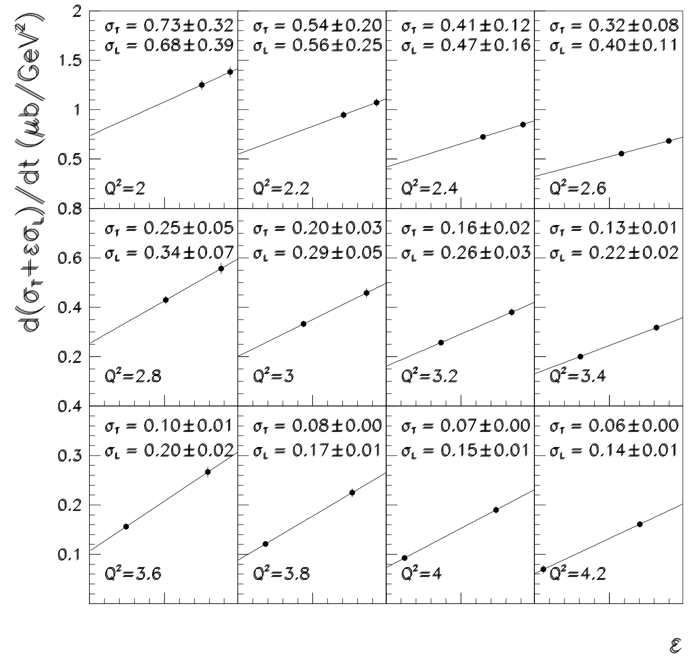

Figure 17: Simulated reconstruction of $d\sigma/dt$ as a function of ϵ for $< x_B >$=0.35 and t=0.3 (GeV/c)^2 for different Q^2 values. The incident beam energies are 6 and 8 GeV. The result of the linear fit yielding σ_T and σ_L is displayed with the associated errors.

One notices two effects : on the one hand, at fixed x_B, as Q^2 increases, the lever arm in ϵ increases and, on the other hand, as Q^2 increases, the count rates decrease. So, in general, relative error bars will first tend to decrease with Q^2 due to the first effect and then increase again, due to the second effect and the low statistics.

The procedure to extract σ_L and σ_T is then to simply apply a straight line to the cross section points obtained at the two ϵ points. The intercept at ϵ=0 yields σ_T, and the slope gives σ_L. Fig. 17 gives the results of the linear fits.

To access higher Q^2 values, the Rosenbluth separation has to be done with 8 and 11 GeV incident energy beams. Figure 18 shows what can be achieved with these two energies. The maximum Q^2 value reachable is then $\approx$ 5.8 GeV^2. The separation is not shown at low Q^2 as it is poor because the lever arm in ϵ is small. To carry out the Rosenbluth separation at low Q^2, lower beam energies are needed.

The results of the fitted σ_T and σ_L cross sections are shown in Fig. 19 along with the existing points of Ref. [20]. This shows that we can carry out an accurate measurement of the separated cross sections up to $Q^2 \approx$5.8 (GeV/c)^2.

4.2 Unseparated cross section for $ep \to en\pi^+$

In the previous section we discussed what kinematics regime can be covered when separating the longitudinal and transverse cross sections. In both cases, $p\rho$ production as well as $n\pi^+$ production the kinematical regime covered is limited to $Q^2 \approx 6$ GeV^2 for a maximum beam energy of 11 GeV. However, the kinematics covered is much larger for the exclusive,

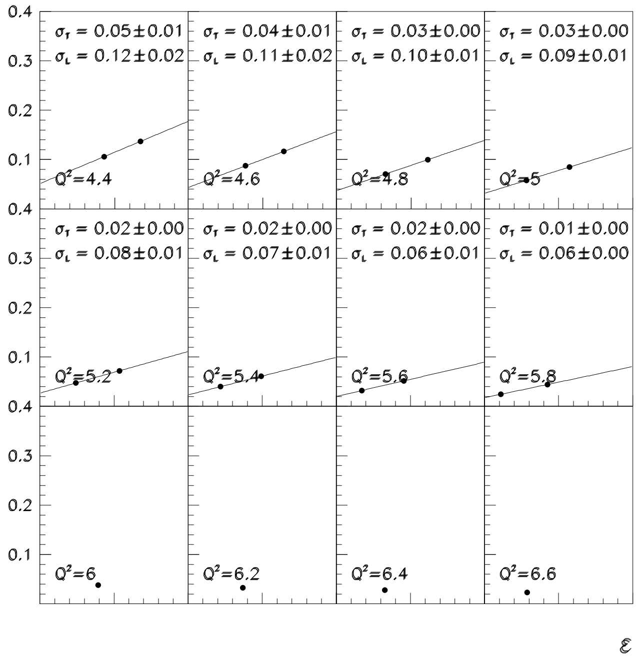

Figure 18: Simulated reconstruction of $d\sigma/dt$ as a function of ϵ for $< x_B >$=0.35 and t=0.3 (GeV/c)^2 for different Q^2 values. The incident beam energies are 8 and 11 GeV. The result of the linear fit yielding σ_T and σ_L is displayed with the associated errors.

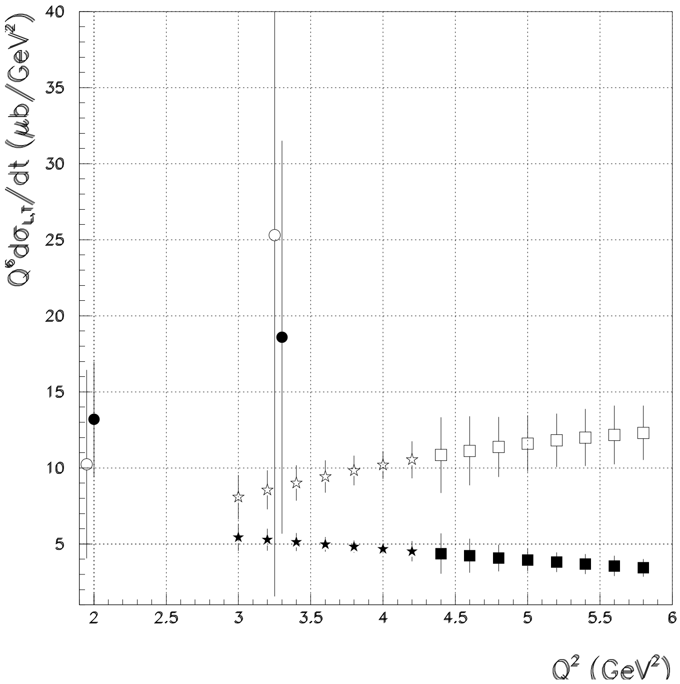

Figure 19: Separated differential cross section $d\sigma/dt$ (multiplied by Q^6) for $\pi^+ n$ as a function of Q^2. The existing data [20] are displayed: open symbols correspond to σ_L and filled symbols to σ_T. The stars are the results of the simulations with 6 and 8 GeV beams (see Fig. 17 and the squares with 8 and 11 GeV beams (see Fig. 18). The circles are the existing data points of Bebek et al. [20].

unseparated cross section. This is shown for the π^+ case in Figure 20. A larger Q^2 range can be covered with significantly smaller error bars. Unseparated cross sections may allow broader access to the GPD if the longitudinal cross section is found to dominate the forward production process. This is indeed expected in $n\pi^+$, as well as in $p\rho^o$. One may expect that corrections to the subleading transverse process may be small enough to be calculable with sufficient accuracy. We note that the L/T separation at smaller Q^2 will provide the testing ground to how accurately these corrections can be controlled.

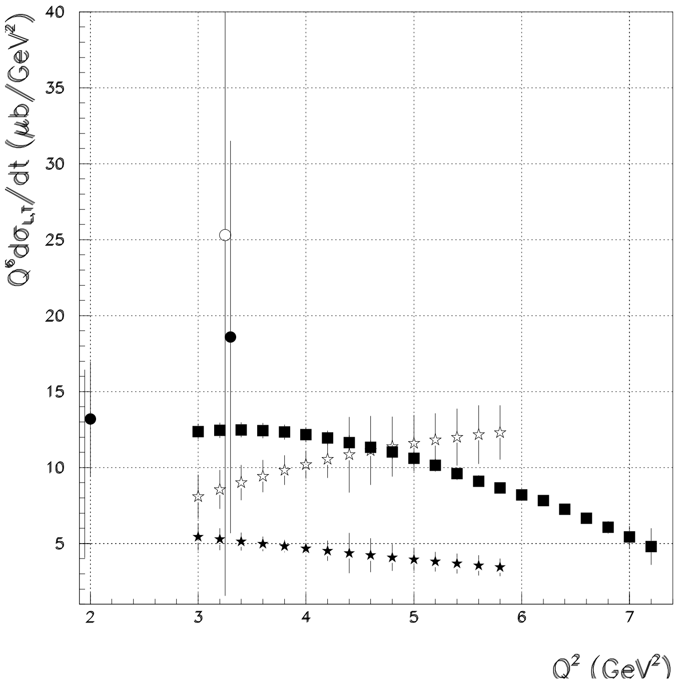

Figure 20: Unseparated differential cross section $d\sigma/dt$ (multiplied by Q^6) for π^+n as a function of Q^2 (full squares), compared to the simulated separated longitudinal and transverse cross sections. The other data points are the same as in Fig. 19.

5 The $ep \to e'(\pi^0, \eta)p$ channel

As was pointed out the x_B dependence of the π^+/π^0 ratio ought to be investigated as the presence of the π^+ pole mechanism in charged-pion electroproduction should yield a peculiar behavior, i.e. an enhancement, in the valence region (see Figure 6).

Also, the comparison of both the π^0 and η (along with the η') cross-sections allows us to perform a flavor separation of the polarized GPDs ($\tilde{H}^u$ and $\tilde{H}^d$) as these GPDs enter with different combinations for these different channels. Recent articles point to the richness of the physics that can be accessed through the neutral pseudoscalar channels. Eides, Frankfurt, and Strikman [?] point out that "It seems likely that a *precocious factorization...* could be valid already at moderately high Q^2 [≥ 5 (GeV/c)^2], leading to *precocious scaling of the spin asymmetries and of the ratios of the cross sections* as a function of Q^2, and x_B". Thus, for example, in the naive quark model they find ratios $\pi^0 : \eta$ of:

$$\frac{1}{2}(\frac{2}{3}\Delta u + \frac{1}{3}\Delta d)^2 : \frac{1}{6}(\frac{2}{3}\Delta u - \frac{1}{3}\Delta d + \frac{2}{3}\Delta s)^2$$

where Δu, Δd, and Δs correspond to the quark-spin helicity distributions. If $\Delta d \approx -\Delta u$ and $\Delta s = 0$, one obtains a ratio of $\pi^0 : \eta = 1{:}3$. This is modified if one includes SU(3) breaking and the axial anomaly, and one gets an x_B dependence when $q\bar{q}$ pairs are included.

6 Deeply Virtual Compton Scattering

Deeply Virtual Compton Scattering (DVCS) is the most promising channel for studying GPD's at lower energies and Q^2. Since there is no hard gluon exchange involved one should expect scaling effects and the validity of the handbag diagram for DVCS starting from $Q^2 \sim 2\ GeV/c^2$ (see discussions in the attached paper by A. Radyushkin [?]). The DVCS process depends on all four GPD's (H, E and $\tilde{H}, \tilde{E}$).

One complication with experimentally studying DVCS is the competing Bethe-Heitler (BH) process. At low energies the BH cross section dominates while with increasing beam energy the relative strength of DVCS increases (see Figure 21), and is predicted to become the dominant contribution at very high energies.

DVCS contributions can be extracted in various ways:

- Direct measurements of the absolute DVCS amplitude in the region where the BH contribution is small and can be calculated
- Extracting the imaginary part of the DVCS amplitude by measuring single-spin asymmetry with longitudinally polarized beam
- Extracting the real part of the amplitude by measuring the beam charge asymmetry

For a complete understanding of GPD's, studies of all three processes are needed in a wide kinematical range. Two can be achieved with electron beams as will be available after the $CEBAF - 12\ GeV$ upgrade, while the third one requires use of positron beams.

Figure 22 shows the cross sections of the DVCS and BH processes as a function of $\theta_{\gamma^*\gamma}$, polar angle between virtual and real photons, for beam energy of 11 GeV. Cross sections are calculated at $Q^2 = 3\ GeV/c^2$ and $X_B = 0.3$ when real photons are produced in the lepton

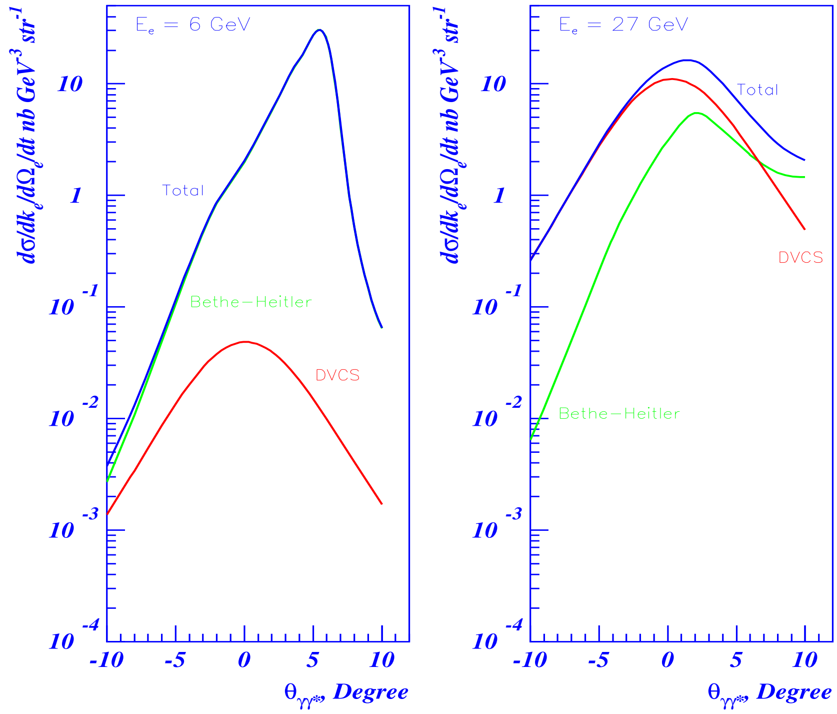

Figure 21: Cross section of $ep \rightarrow ep\gamma$ as a function of the angle between virtual and real photons at beam energies 6 GeV and 27 GeV. Kinematics of the reaction was fixed at $Q^2 = 3\ GeV/c^2$ and $X_B = 0.3$. Red curve is the contribution of DVCS, green curve is Bethe-Heitler and blue curve is the total. Cross sections are calculated according to [27].

scattering plane [27]. In the range of $\theta_{\gamma^*\gamma} > -2.5^o$ the BH contribution is dominant in the total cross section, while at $\theta_{\gamma^*\gamma} < -5^o$ $(-t > 0.4\ GeV/c^2)$ the DVCS contribution dominates the cross section.

6.1 Electron spin asymmetries

The availability of highly polarized electron beam will allow the measurement of beam spin asymmetries. These arise as the result of interference terms between real and imaginary parts of longitudinal and transverse amplitudes. Figure 23 shows the predicted asymmetry for $t = 0.3\ GeV/c^2$ and $X_B = 0.2$ and $X_B = 0.3$ at $Q^2 = 3\ GeV/c^2$. One expect about 40% asymmetry in these cases.

The re-designed CLAS detector in Hall-B is well suited to conduct the proposed studies. Figure 24 shows the kinematical range in Q^2 and W accessible with CLAS [28] for beam energy of 11 GeV. Systematic studies in the range of Q^2 up to 6 GeV/c^2 and X_B from 0.15 to 0.45 will be possible.

Another important parameter is the transferred four-momentum to the hadronic system, t. The coverage in t (or polar angle of scattered photon respect to the virtual photon) is defined by the detection of the photon and/or the proton in the final state. Figure 25 shows the kinematics of the final state photons and protons in the reaction $ep \rightarrow ep\gamma$ for 11 GeV beam energy. Electrons are selected in the ϕ range from -30^o to 30^o, Q^2 is fixed at 3 GeV/c^2 and $X_B = 0.3$. Both particles are in the acceptance range of CLAS (see also discussions in the next session).

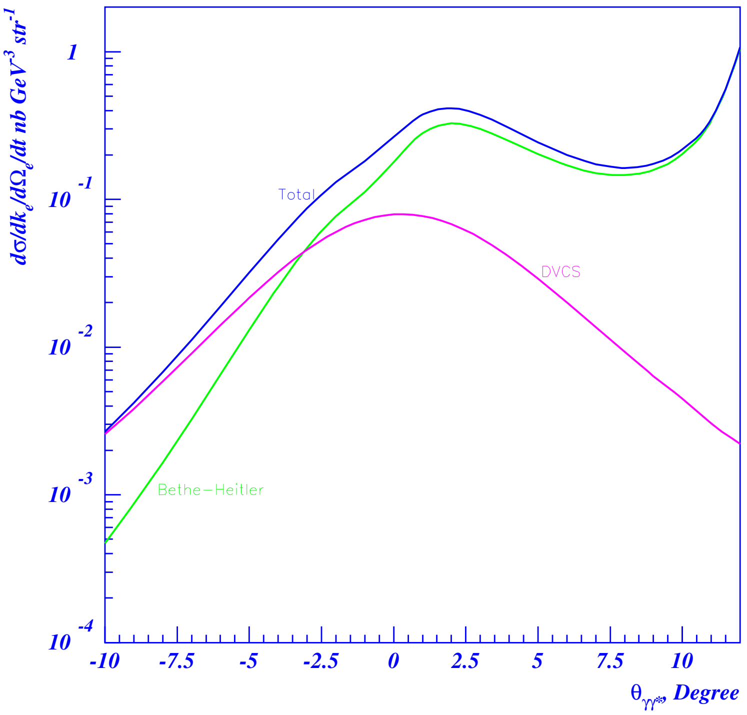

Figure 22: Cross section of $ep \to ep\gamma$ as a function of the angle between virtual and real photons at beam energy 11 GeV, $Q^2 = 3\ GeV/c^2$ and $X_B = 0.3$.

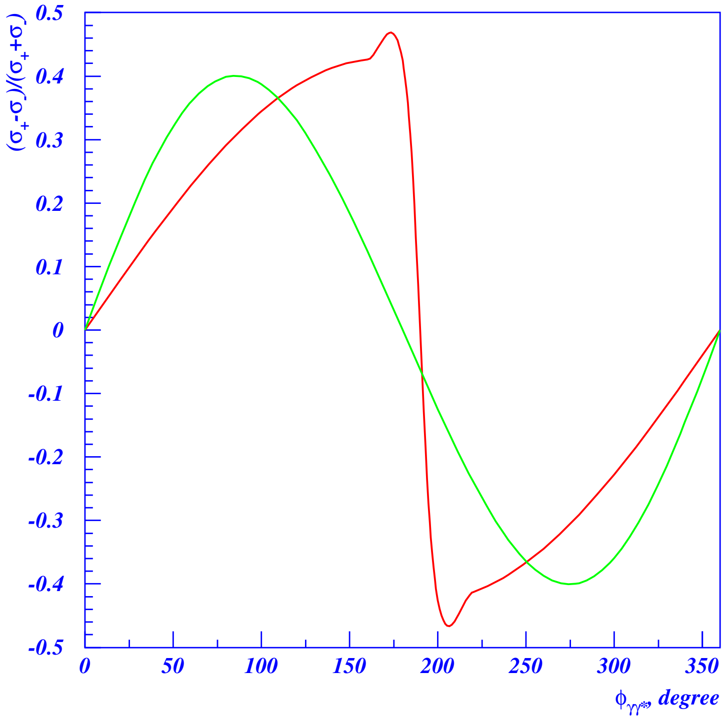

Figure 23: Predicted single spin asymmetry with longitudinally polarized 11 GeV electron beam. (a) asymmetries for $-t = 0.3\ GeV/c^2$ at $X_B = 0.2$, green curve, and $X_B = 0.3$, red curve. (b) the same for $-t = 0.5\ GeV/c^2$. Calculations according [27].

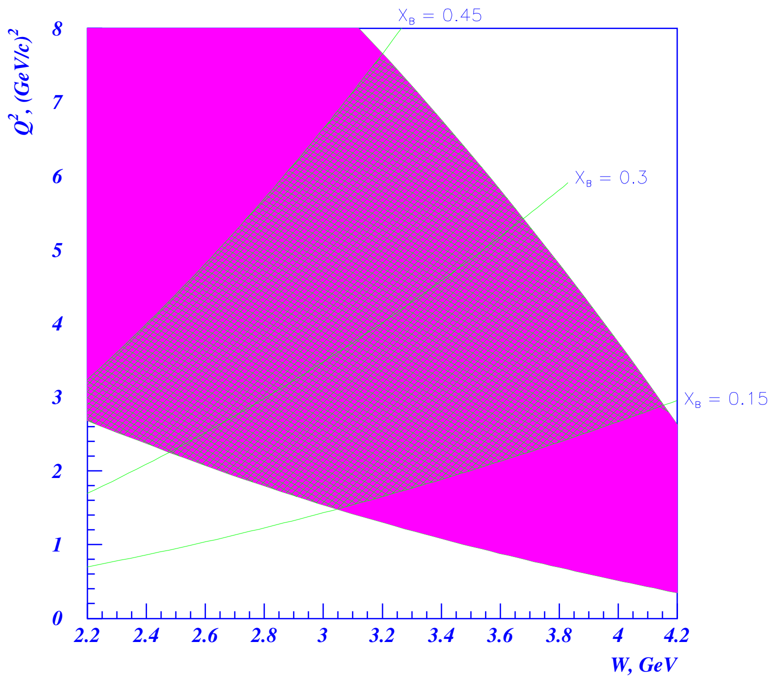

Figure 24: The accessible range of Q^2 and W at 11 GeV beam energy with new design of CLAS detector. Full read region is defined by scattered electron detection. Green shaded region is the favorable kinematical range, accessible for DVCS measurements. Green lines represent fix values of X_B.

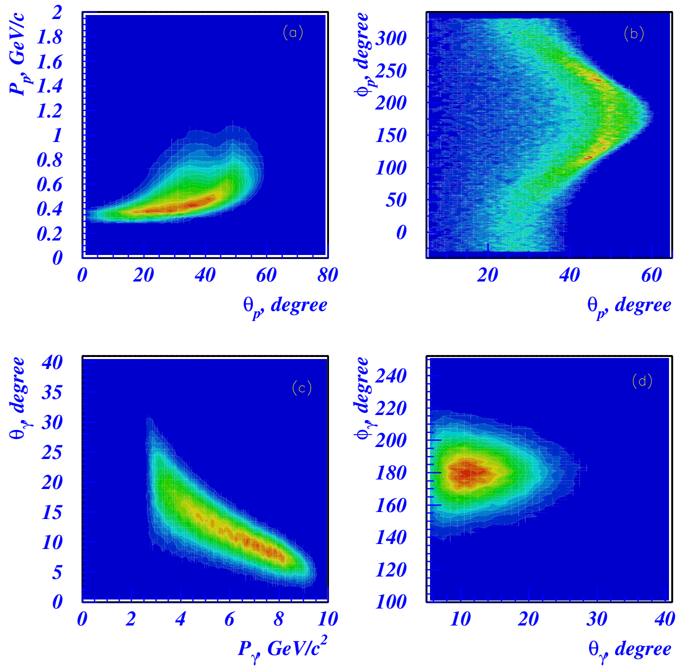

Figure 25: Kinematics of scattered photon and recoil proton in the reaction $ep \rightarrow ep\gamma$ with 11 GeV beam. Electron was fixed at $Q^2 = 3\ GeV/c^2$, $X_B = 0.3$ and the azimuthal angle between -30^o and 30^o.

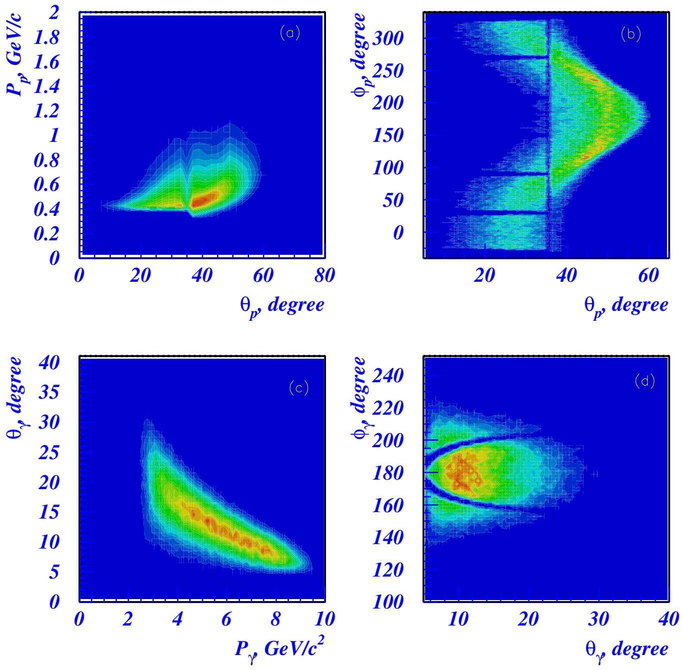

Figure 26: Momentum and angular distributions of detected protons, (a) and (b), and photons, (c) and (d). Acceptance for protons in the forward region ($\theta < 35^o$) is defined by CLAS torus. At large angles full efficiency for protons from $0.2GeV/c$ to $2GeV/c$ is assumed. Gap in the order of 1^o is introduced as transition from forward to the backward part of the detector. Photons are detected in the present forward electromagnetic calorimeter of CLAS and in the proposed compact calorimeter under the shadow of torus coils. Gaps between different modules are introduced for possible edge effects on the forward calorimeter.

6.2 Experimental aspects of DVCS and π^o production

At high energies, the missing mass technique, though still useful, will be insufficient to separate single photon from π^o production, if only scattered electron and recoil proton are measured in the reaction $ep \rightarrow epX$. Fully exclusive or semi-exclusive measurements will be needed to uniquely identify the exclusive reaction. Since experimental signatures of DVCS and deeply virtual π^o production are the same, and one is the background process for the other one, both reactions must be studied, simultaneously. In case of DVCS and π^o production, the final state $ep\gamma$ can be used to separate the two processes.

Simulation of both, DVCS and π^o electroproduction have been performed using a realistic parameterization of the CLAS detector acceptance with the proposed new design [28]. Detector performance at high energies for the forward region $\theta < 35^o$ is extrapolated from existing experimental measurements and GEANT simulations. For photon and charge hadron detection in the angular range from $\theta = 36^o$ to $\theta = 100^o$ a fully efficient detector, with complete azimuthal coverage, in the momentum range of $0.2GeV/c < p < 2GeV/c$ is assumed.

Momentum and angular distributions of the detected protons are presented in Figure 26a,b. In the forward scattering region, $\theta < 35^o$, the acceptance is defined by the CLAS torus, while in the large angle scattering region, where a new inner detector package is proposed to be installed [28], every proton is accepted within an angular range $\theta = 36^o$ to 100^o.

The high energy photons are produced predominantly in the forward region and therefore

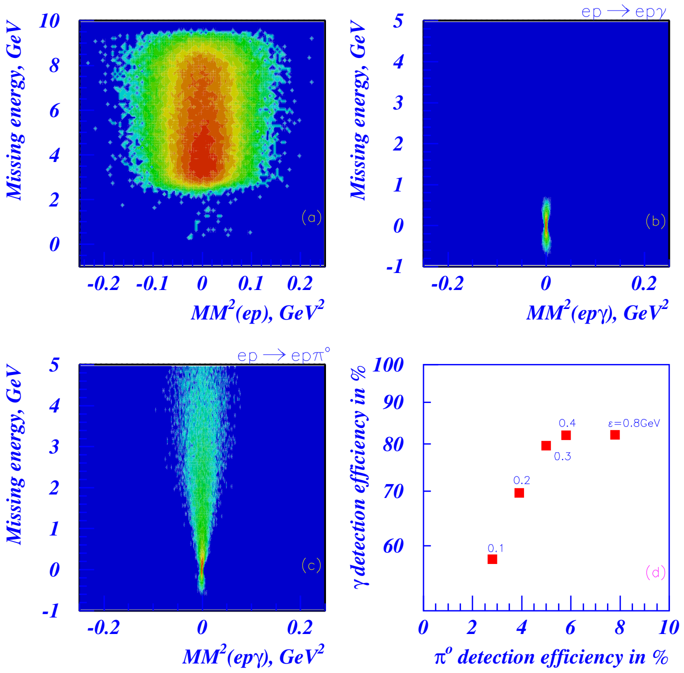

Figure 27: Missing mass and missing energy cuts for $ep \rightarrow ep\gamma$ and $ep \rightarrow ep\pi^o$ separation in the $ep\gamma$ final state. (a) missing mass vs missing energy for (ep) final state in the reaction $ep \rightarrow ep\gamma$. (b) and (c) are the missing mass vs missing energy for the $ep\gamma$ final state for reactions $ep \rightarrow ep\gamma$ and $ep \rightarrow ep\pi^o$, respectively. Plot (c) is the efficiency of the reconstruction of individual channel in the ($ep\gamma$) final state for different missing energy cut.

detection of photons will be done mainly in the existing forward electromagnetic calorimeter with improved position resolution. However there is significant acceptance loss due to torus coils and this loss is large especially in the very forward region where coils are covering much of the phase space. In the new CLAS design compact electromagnetic calorimetry is implemented in the inner-forward part of the detector to cover the shadow region of the coils. This will result in a significant improvement of the detection efficiency for photons in the forward scattering region. Figure 26c,d shows the momentum and angular distributions of detected photons. Effects of the new coil calorimeters are clearly seen in Figure 26d. There are still small gaps between different sections that represent a loss of efficiency due to possible edge effects.

Deep virtual π^o production will be the main source of background for $ep \rightarrow ep\gamma$. Since pions have momenta up to 9 GeV/c, the current granularity of CLAS forward calorimeter will not be sufficient for resolving individual photons from π^o decay. In the proposed new design, CLAS has a preshower detector before the forward electromagnetic calorimeter, with finer segmentation. This will allow resolving two photons from high energy π^o decay. In simulations, fully efficient detection of the each photon in the calorimeters is assumed. Figure 27 shows the distribution of missing mass and missing energy, and the efficiency of the separation of $ep \rightarrow ep\gamma$ and $ep \rightarrow ep\pi^o$ reactions.

A simple, one dimensional cut on missing energy is already sufficient to discriminate between single photon and π^o productions. One needs to note that cuts on angles of the missing system will be used as well, which will give additional improvement in identifying the reaction.

It is also clear from Figure 27, that selecting events with small or large missing energy will effectively select reaction $ep \rightarrow ep\gamma$ or $ep \rightarrow ep\pi^o$, respectively. The value of the

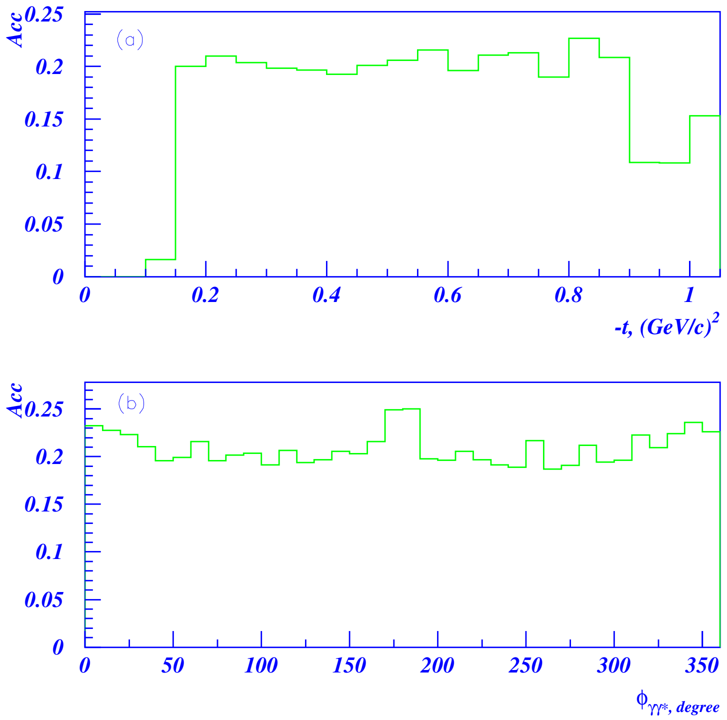

Figure 28: CLAS acceptance as function of transfered momentum (upper plot) and as a function of the ϕ angle between lepton plane and the real photon scattering plane.

missing energy cut must be defined from experiment after estimation of relative yields of these reactions. For these studies, detection of the two photons from π^o decay can be used. At these kinematics in 30% of all cases two the photon are detected in the calorimeters.

6.3 Count rates

As mentioned earlier, to extract information on the GPD's from DVCS measurements using a highly polarized electron beam at 11 GeV, we propose to employ two possibilities. First, the direct measurements of DVCS cross section (square of DVCS amplitude) in a wide range of Q^2, X_B, and t, in the kinematics where contribution from DVCS is larger than from the Bethe-Heitler process. Second, the measurements of single spin asymmetry as a function of the ϕ angle between lepton plane and the real photon scattering plane.

For these two measurements, count rates are estimated using the cross sections calculated by [27]. We assume that CLAS will be capable of running at a luminosity of $L = 10^{35}\ cm^{-2}\ sec^{-1}$. Detector acceptances were derived from simulations described above.

Figure 28 shows the detection efficiency for the $ep\gamma$ final state in the kinematical range of the proposed measurements. Efficiencies of $\sim$ 20% are achieved independent of the transfered momentum and $\phi_{\gamma^*\gamma}$. (The loss of acceptance at $t < 0.15\ GeV/c^2$ is due to the inefficiency of the detector to the low energy protons. Depletion in the high t range is mainly due to photons lost in the forward hole.)

In Figure 29 we show the cross section of the reaction $ep \rightarrow ep\gamma$ as a function of t. Errors are projected for 500 hours of running CLAS at luminosity $10^{35}\ cm^{-2}\ sec^{-1}$. Electron kinematics is fixed in the ranges $Q^2 = 3 \pm 0.1\ GeV/c^2$ and $X_B = 0.3 \pm 0.025$. Photons are selected in the range of azimuthal angle $\phi_{\gamma^*\gamma} = 0 \pm 10^o$. In this ϕ range for

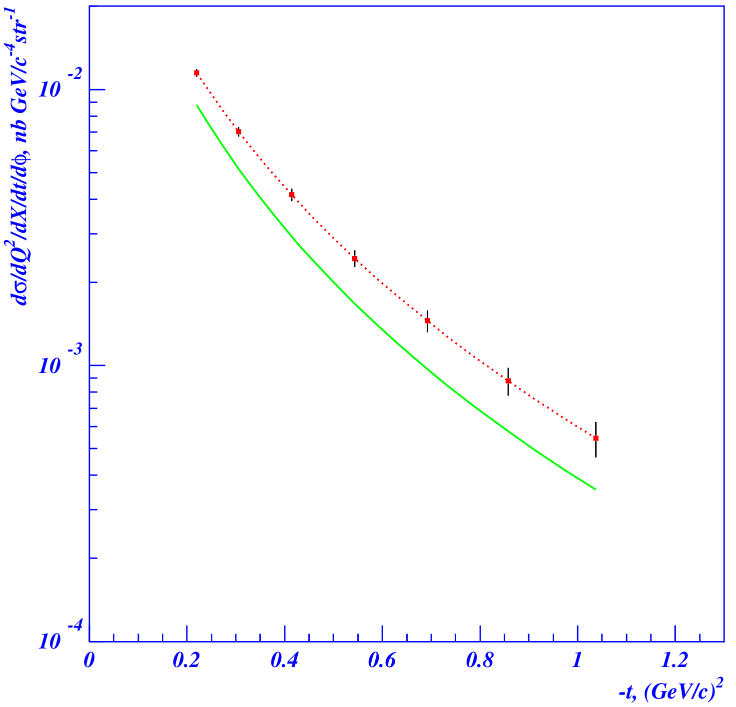

Figure 29: t-dependence of the cross section of $ep \rightarrow ep\gamma$ process at beam energy 11 GeV. Errors are evaluated according to 500 hours of running CLAS at luminosity 10^{35} cm^{-2} sec^{-1}. Pseudo data were integrated in the bins of $Q^2 = 3 \pm 0.1$ GeV/c^2 and $X_B = 0.3 \pm 0.025$ and $\phi_{\gamma^*\gamma} = 0 \pm 10^o$.

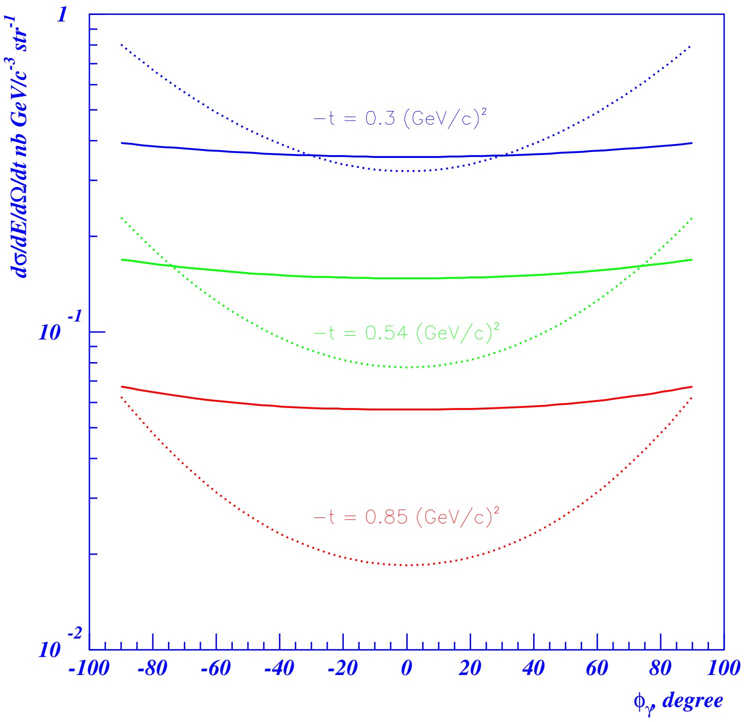

Figure 30: ϕ-dependence of the contributions of DVCS (solid curve) and BH (dashed curve) process at beam energy of 11 GeV for different transfered momenta.

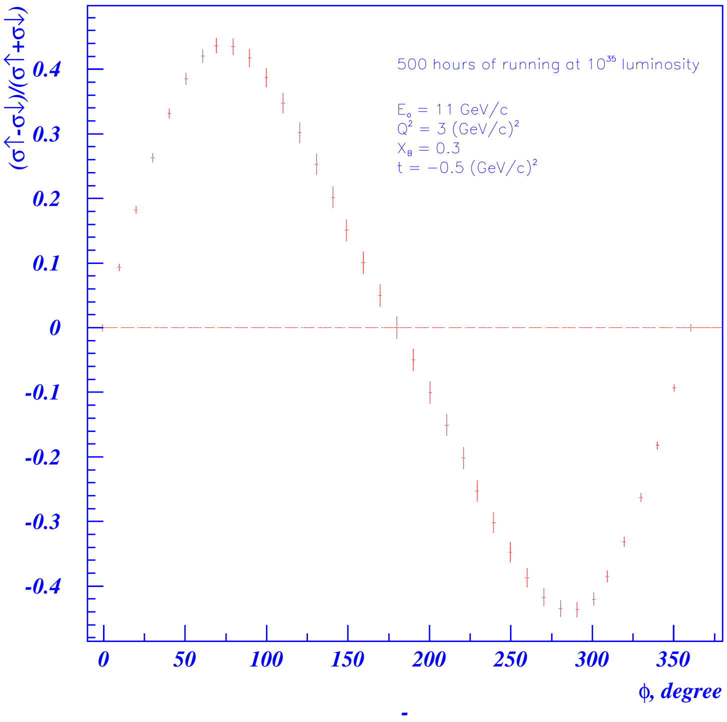

Figure 31: Single spin asymmetry of the cross sections of $ep \rightarrow ep\gamma$ reaction measured with longitudinally polarized 11 GeV electron beam. Errors correspond to 500 hours of running on CLAS at luminosity 10^{35} cm^{-2} sec^{-1}. Pseudo data were integrated in the bins of $Q^2 = 3 \pm 0.1$ GeV/c^2 and $W = 2.8 \pm 0.15$ GeV and $-t = 0.3 \pm 0.1$ GeV/c^2.

$-t > 0.3$ GeV/c^2 DVCS contribution is larger than contribution from Bethe-Heitler process (see Figure 30).

Similar estimations of the expected statistical errors for measurements of beam spin asymmetries with longitudinally polarized beam have been done as well. In Figure 31 the asymmetries are shown with projected (statistical) errors for 500 hours of running CLAS in the same conditions as above.

7 Polarized Target Spin Asymmetry

Single target spin asymmetries in single pion production provide yet another handle on the GPD. These asymmetries depend on imaginary parts of products of the integrals of the $\tilde{H}$ and $\tilde{E}$ GPD, as shown in more detail in the next section.

We estimate the error bars obtained with a 2000 hours measurement using a polarized NH_3 target at a luminosity of $10^{35} cm^{-2}s^{-1}$. The target would be placed in the 5 Tesla solenoid magnetic field. Positive pions are detected in the upgraded CLAS in coincidence with the scattered electron.
The reaction of interest

$$ep \rightarrow e'\pi^+ n$$

can be identified and separated from excitation processes such as the $ep \rightarrow e\Delta^o(1232)$ using missing mass cuts. This procedure has been successfully used at energies up to 5.5GeV in unpolarized experiments, and will be used this fall at energies up to 5.7GeV in a polarized target experiment E-93-036 using a NH_3 target in CLAS. Simulations show that with the proposed CLAS upgrade this methods can be extended to the 11 GeV available after the CEBAF energy upgrade.

The precision that can be achieved in the asymmetry extraction depends on the target polarization and dilution factor that represent the fraction of polarized nucleon in the target. Target polarization, according to our experience, was assumed 90% and dilution factor was fixed to 0.4. This value results from the analysis of the same reaction using a polarized NH_3 target in CLAS at lower energies. It is larger than that normally obtained in inclusive experiments where contribution from protons and neutrons can not be separated, because the proposed exclusive reaction channel is sensitive mostly to proton contribution. We consider that the presence of a transverse polarized target would be of high importance to carry out a detailed exclusive polarized target program, however, for the purpose of this estimate we have assumed a longitudinally polarized target as is presently installed in Hall B. In fact, within the proposed kinematical range, a target polarized longitudinally to the electron beam has a significantly non-zero polarization component transverse to the virtual photon ranging from 10% at low Q^2 and low x_{Bj} up to 36% at higher Q^2 and low x_{Bj}. Acceptance studies show that good statistics can be achieved in the Q^2 interval $2 - 4GeV^2/c^2$ and in the x_{Bj} interval $0.2 - 0.4$, corresponding to $W > 2GeV$, and consequently, that a study of the Q^2 dependence of the asymmetry in a wide x_{Bj} interval can be performed. Although the Q^2 range covered in this measurement will be smaller than in unpolarized pion production, it will, for example, allow the testing of the proposed precocious scaling behavior.

In fig. **??** we report the projected statistical error for three different t values and $x_{Bj} = 0.35$ assuming a $\Delta x_{Bj} = 0.1$, $\Delta Q^2 = 0.4GeV^2/c^2$ and $\Delta t = 0.1GeV^2$ binning.

In fig 33 comparison with theoretical expectations are shown for different Q^2 values. Considering evaluations from ref. [10] where the asymmetry for the reaction

$$ep \rightarrow e'\pi^+ n$$

has been estimated for different assumptions for the asymptotic pion distribution amplitude. Sufficient sensitivity is achieved to discriminate between different models.

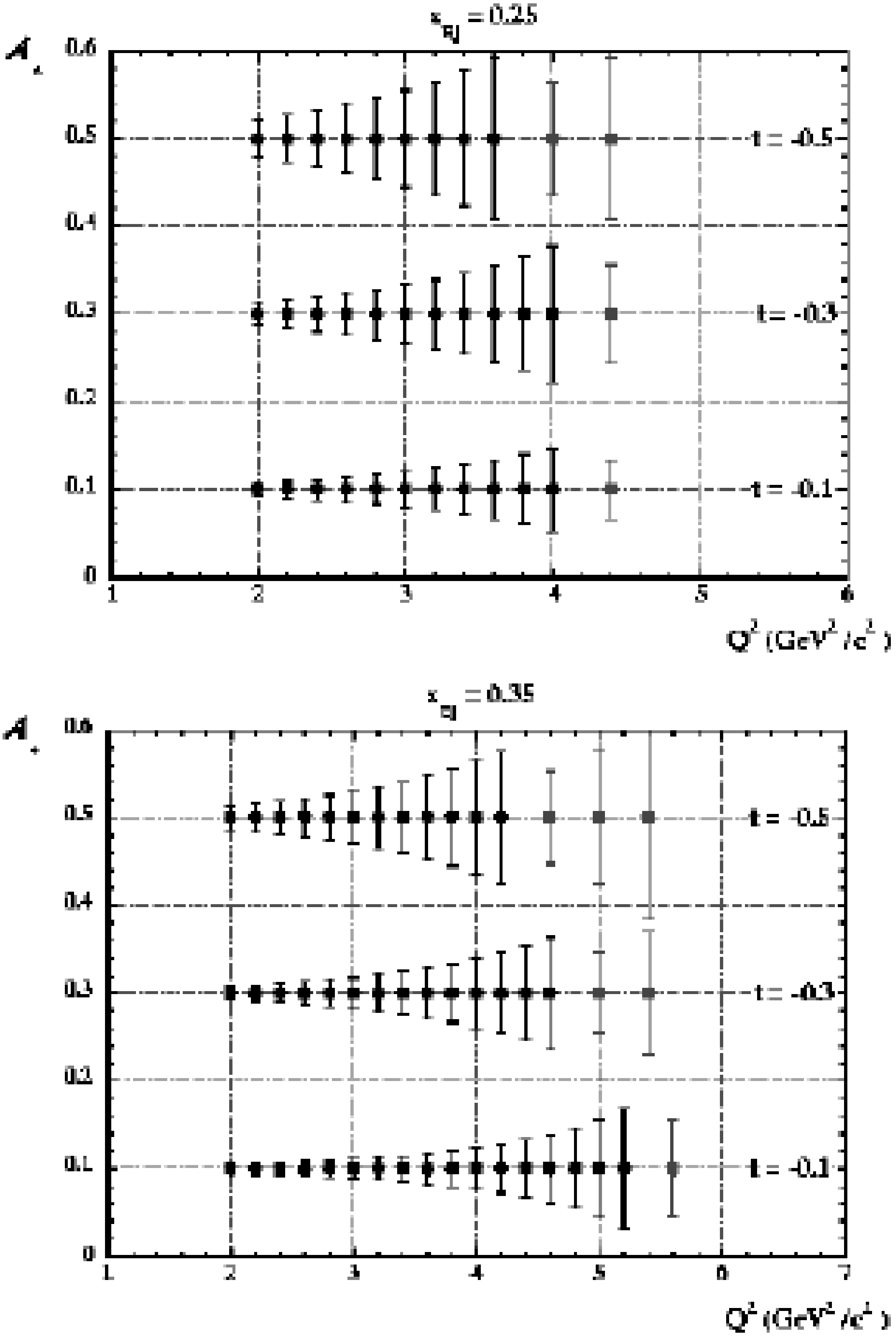

Figure 32: Estimated errors on the transverse target spin asymmetry for different values of x_{Bj} and t, versus Q^2
.

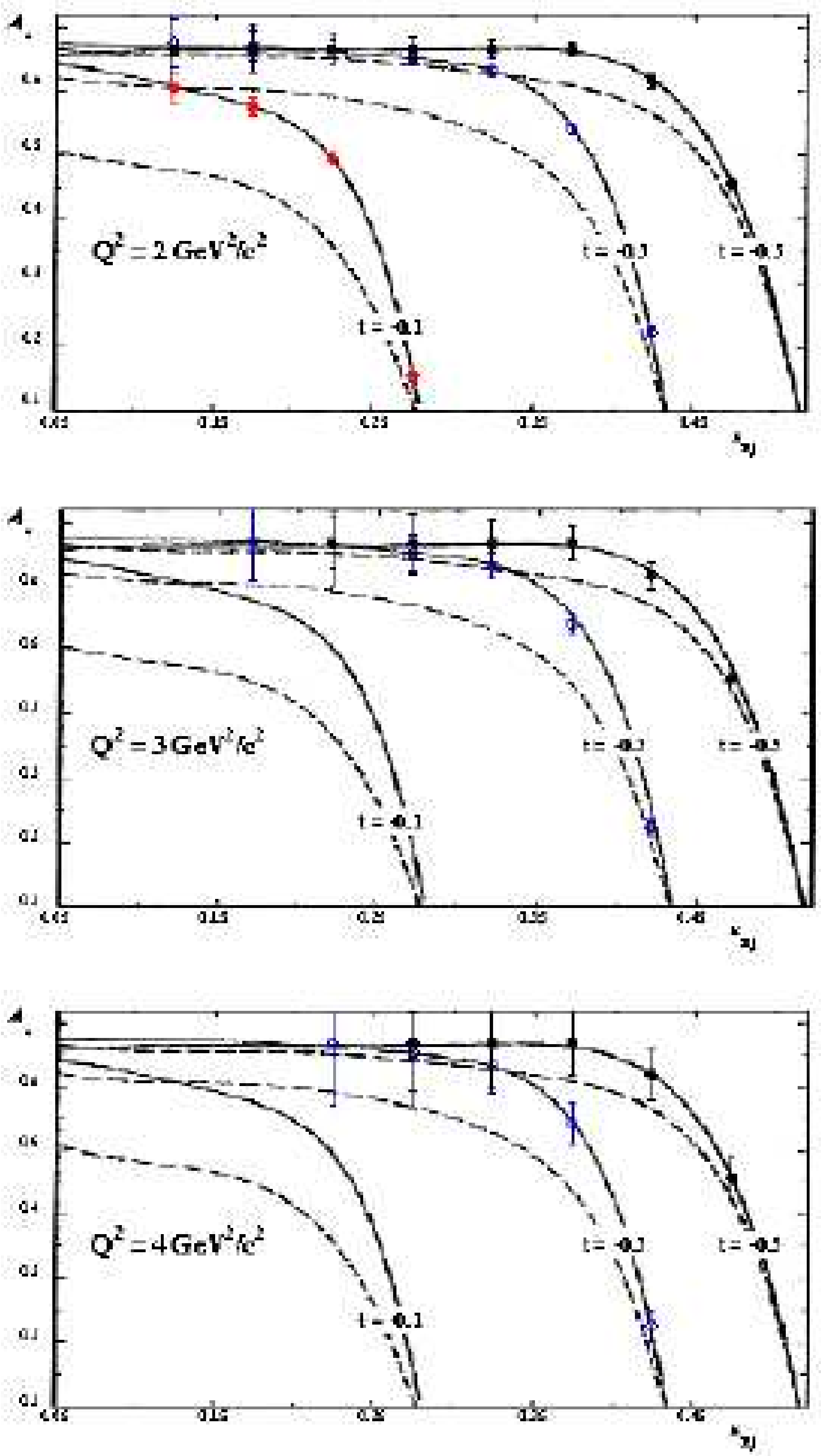

Figure 33: The transverse target spin asymmetry for different values of Q^2 as a function of x_{Bj}. The solid and dashed curves represent different model assumption regarding the GPD's.

8 Sensitivities of observables to various models of GPD's

8.1 General remarks about relations between observables and GPDs

We first review the relations between the observables that can be measured in the proposed experiments (differential cross sections, beam and target asymmetries) and the way the GPDs enter into them. The leading order amplitudes for vector meson (VM), pseudo-scalar meson (PS) production and DVCS on the nucleon can be written as :

$$\mathcal{M}^L_{VM} \propto \frac{1}{Q}\left[\int_0^1 dz \frac{\Phi_{VM}(z)}{z}\right] \int_{-1}^{+1} dx \left[\frac{A}{x-\xi+i\epsilon} + \frac{B}{x+\xi-i\epsilon}\right] \times \left\{H(x,\xi,t)\bar{N}(p^{'})\gamma.nN(p) + E(x,\xi,t)\bar{N}(p^{'})i\sigma^{\kappa\lambda}\frac{n_\kappa \Delta_\lambda}{2m}N(p)\right\}, \quad (6)$$

$$\mathcal{M}^L_{PS} \propto \frac{1}{Q}\left[\int_0^1 dz \frac{\Phi_{PS}(z)}{z}\right] \int_{-1}^{+1} dx \left[\frac{C}{x-\xi+i\epsilon} + \frac{D}{x+\xi-i\epsilon}\right] \left\{\tilde{H}(x,\xi,t)\bar{N}(p^{'})\gamma.n\gamma_5 N(p) + \tilde{E}(x,\xi,t)\bar{N}(p^{'})\gamma_5\frac{\Delta\cdot n}{2m}N(p)\right\}, \quad (7)$$

$$\begin{aligned}
&\mathcal{M}^T_{DVCS} \\
\propto\ & K\int_{-1}^{+1} dx \left[\frac{1}{x-\xi+i\epsilon} + \frac{1}{x+\xi-i\epsilon}\right] \\
&\times\left[H(x,\xi,t)\ \bar{N}(p^{'})\gamma.nN(p) +\ E(x,\xi,t)\ \bar{N}(p^{'})i\sigma^{\kappa\lambda}\frac{n_\kappa\Delta_\lambda}{2m}N(p)\right] \\
+\ & L\int_{-1}^{+1} dx \left[\frac{1}{x-\xi+i\epsilon} - \frac{1}{x+\xi-i\epsilon}\right] \\
&\times\left[\tilde{H}(x,\xi,t)\bar{N}(p^{'})\gamma.n\gamma_5 N(p) + \tilde{E}(x,\xi,t)\bar{N}(p^{'})\gamma_5\frac{\Delta\cdot n}{2m}N(p)\right], \qquad (8)
\end{aligned}$$

where most of the symbols are defined in section 2.

We first note some basic points :

- In equations 6 and 7, $\Phi_{VM,PS}(z)$ is the meson distribution amplitude which can, at this stage, be considered as basically known (asymptotic shape $\propto z(1-z)$, see for example [24]). Of course, it does not appear in the DVCS amplitude.
- In equations 6 and 7, the factor $\frac{1}{Q}$ in front the amplitude originates from the gluon exchange in the diagrams of figure 7. It is not present for the DVCS amplitude (figure 2). This factor makes the differential cross section for mesons scale as $\frac{1}{Q^6}$ for meson production and $\frac{1}{Q^4}$ for DVCS (see figure 3), when taking into account the squaring of the amplitude and the phase space factor.
- One sees that the vector meson amplitude is proportional only to the unpolarized GPDs (H and E), the pseudoscalar meson amplitude only to the polarized GPDs ($\tilde{H}$ and $\tilde{E}$) and the DVCS amplitude to both.

- The coefficients A, B, C, D are different according to the isospin channels : see table 1 for some typical examples.

- The GPDs are actually defined for each quark flavors. According to the produced particle, the decomposition onto the quarks flavors is different : see table reftab:isospin2 for the numerical coefficients.

- The factorization theorem, which allows parametrization of the nucleon structure in terms of GPDs, only applies to the longitudinal part of the electromagnetic current for mesons, and to the transverse part of the current for DVCS. In their respective channels, both these contributions are predicted to dominate at asymptotically large Q^2. In other words, we can consider that, for mesons, at leading order, transverse currents can be approximated to 0 (at least suppressed) and that, for Compton, longitudinal currents are suppressed. This means that, for mesons, only observables involving <u>longitudinal</u> currents are relevant for our studies. There are only 2 such observables ; the longitudinal unpolarized cross section (which therefore requires a L/T separation) and the transverse spin target asymmetry. We will detail these below. Similiarly, for DVCS, a priori, only observables involving <u>transverse</u> currents should be relevant. We will however see below that, due to the well known Bethe-Heitler process, which leads to the same final state as DVCS, interferences can occur and LT interference response functions such as the beam asymmetry are also of great interest.

- The amplitudes have both a real and an imaginary part.

	A	B	C	D
ρ^0	1	1	0	0
ρ^+	-2/3	1/3	0	0
ρ^-	-1/3	2/3	0	0
ω	1	1	0	0
π^0	0	0	1	1
π^+	0	0	-2/3	1/3
π^-	0	0	-1/3	2/3
η	0	0	1	1

Table 1: Coefficients A, B, C, D of Eq. 6 and 7 for different isospin channels.

We now come to the observables relevant for mesons channels. We start with the longitudinal differential cross section which is related to the amplitude through :

$$\frac{d\sigma_L}{dt} \propto \frac{1}{2}\sum_{h_N}\sum_{h_N^{'}} |\mathcal{M}^L(\lambda_M = 0, h_N^{'}; h_N)|^2 \tag{9}$$

One therefore sees that, when measuring a cross section, one will actually measure the square of an integral (over x) of the GPD's (for instance, by dropping the $\frac{1}{x+\xi+i\epsilon}$ and the E GPD terms with respect to equation 6 for sake of clarity, one roughly measures $\int_{-1}^{+1} dx \frac{H(x,\xi,t)}{x-\xi+i\epsilon}$ in ρ^0 production). Also, the differential cross section is sensitive to both the real and the imaginary part.

	H^u	H^d	$\tilde{H}^u$	$\tilde{H}^d$
ρ^0	$\frac{2}{3\sqrt{2}}$	$\frac{1}{3\sqrt{2}}$	0	0
ρ^+	1	-1	0	0
ρ^-	1	-1	0	0
ω	$\frac{2}{3\sqrt{2}}$	$\frac{-1}{3\sqrt{2}}$	0	0
π^0	0	0	$\frac{2}{3\sqrt{2}}$	$\frac{1}{3\sqrt{2}}$
π^+	0	0	1	-1
π^-	0	0	1	-1

Table 2: Decomposition of the GPDs on the quark flavors for different channels.

Now, we look at the transverse spin target asymmetry. In terms of amplitudes, the transverse spin target (longitudinal) response function $\sigma_L^\perp$ is defined as :

$$\sigma_L^\perp \propto \frac{1}{2} \sum_{h'_N} 2Im(\mathcal{M}^L(\lambda_M = 0, h'_N; +1/2) \times \mathcal{M}^L(\lambda_M = 0, h'_N; -1/2)^*) \tag{10}$$

The corresponding transverse spin target asymmetry is then, directly in terms of (polarized) GPDs (which is relevant for pseudoscalar mesons. A similar expression holds for the unpolarized GPDs accessed through vector meson production, by replacing $\tilde{H}, \tilde{E}$ by H, E up to some kinematical factors) :

$$\begin{gathered} \mathcal{A} = \tfrac{|\Delta_\perp|}{\pi m_N} \, \tfrac{2\xi \, Im(FG^*)}{D} \, , \\ D = |F|^2(1-\xi^2) - |G|^2 \, \tfrac{\xi^2 t}{4m_N^2} - 2\xi^2 Re(FG^*) \end{gathered} \tag{11}$$

F and G being given by :

$$F = \int_{-1}^{1} dx \, \tilde{H}(x,\xi,t) \left\{ \frac{A}{x-\xi+i\epsilon} + \frac{B}{x+\xi-i\epsilon} \right\}, \tag{12}$$

$$G = \int_{-1}^{1} dx \, \tilde{E}(x,\xi,t) \left\{ \frac{A}{x-\xi+i\epsilon} + \frac{B}{x+\xi-i\epsilon} \right\} \tag{13}$$

This shows that this observable is proportional to the product of the (integrals over x) of the $\tilde{H}$ and $\tilde{E}$ GPDs (similarly for the H and E GPDs). This is extremely important as this allows access to the E GPD for instance (E is actually the least known of the 4 GPDs and one of the most important as it enters the Ji's orbital momentum sum rule). Indeed, the differential cross section is not very sensitive to the E GPD as there is a factor Δ ($t = \Delta^2$) in front of it (see Eq. 6) which kinematically suppresses its contribution at forward angles. Also, it enters in quadrature with the H GPD when squaring the amplitude for the differential cross section whereas, here, the transverse spin target asymmetry is linearly proportionnal to E.

For DVCS, the relevant current is the transverse one. For the differential cross section, we therefore have to measure the transverse one $\frac{d\sigma_T}{dt}$. In principle, an L/T separation should also be needed here. However, there are reasons to believe that the transverse cross section is dominant for DVCS already at small Q^2 values, which should spare us the task of separating the L and T contributions. First, we already know that at Q^2=0 (photoproduction), the cross section is purely transverse (This is a difference with the mesons where the relevant current to isolate is the longitudinal one which is obviously not dominant at Q^2=0). So, DVCS has already a "good start" at small Q^2. Second, we know that in inclusive DIS (which is essentially the "diagonal" image of DVCS) the transverse current is the dominant one in the hard scattering. Hard scattering (Bjorken regime) in DIS has been measured down to $Q^2 \approx 1$ GeV^2 which bears evidence to the dominance of the transverse current to such low Q^2. As a last argument, the outgoing photon being real and therefore transverse, production by a longitudinal virtual photon must be suppressed as it would have to be a helicity-flip amplitude.

Therefore, we have all reasons to believe that a L/T separation is not needed for DVCS and that the transverse current is the dominant one already at low Q^2 values. So, for DVCS, we will measure the differential cross section, considering it as purely transverse, and therefore proportional to the GPDs in the same fashion as for mesons, i.e. involving the integral (over x and weighted by factors $\frac{1}{x \mp \xi \pm i\epsilon}$) of the GPDs. As the A, B, C and D coefficients of Eq. 6 and 7 are different from the mesons channels, we gain extra information for the separation of the GPDs and their decomposition into the quark flavors. Besides, one of the main advantage of DVCS is that, in similarity to the process with DIS, we expect the onset of the Bjorken regime at smaller Q^2 than for mesons. The reason is that there is no gluon exchange involved in leading order DVCS, in contrast with meson production where "soft" Feynman mechanisms can dominate the leading order 1-gluon exchange mechanism (which we are after) at low Q^2.

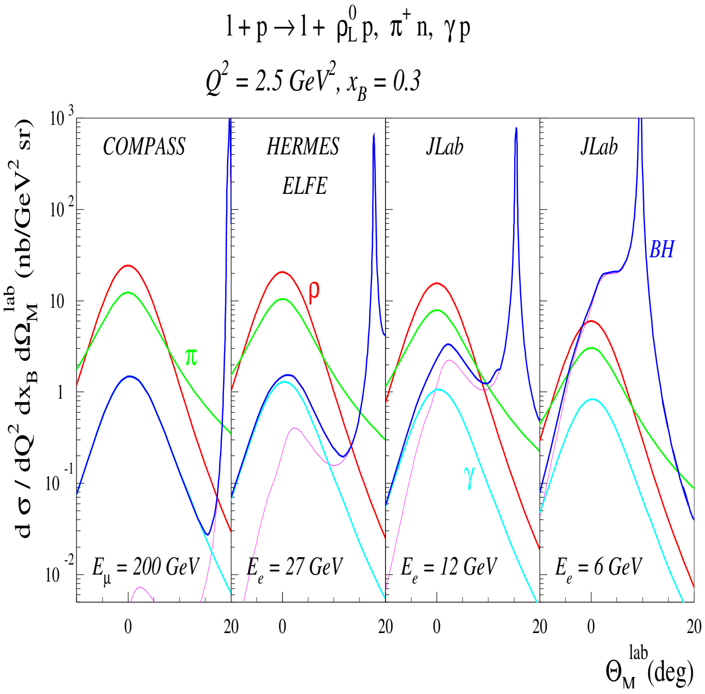

Figure 34: Longitudinal (for mesons) and transverse (from Compton) differential cross section $d\sigma/dt$ for ρ^0, $\pi^+ n$ and γ electroproduction on the prootn as a function of $theta_{lab}$ (scattering angle of the meson or photon in the laboratory) for different beam energies. For the photon channel, the DVCS, the Bethe-Heitler alone, and the sum of the 2 processes are distinguished.

A competing mechanisn to DVCS is the Bethe-Heitler (BH), i.e. the radiation a photon by the (incoming or outgoing) electron. It leads to the same final state as DVCS (where the photon is emitted from the nucleon). Figure 34 shows that the relative importance of BH with respect to DVCS varies with the incident beam energy and with the scattering angle of the photon (it also varies with x_B). From this figure, it is clear that it would extremely difficult to access pure DVCS with a 6 GeV beam energy where the cross section is completely dominated by BH in most of the kinematical range.

However, at 11 GeV, as shown in figure 34, there is a window ($\Phi = 180^o$, scattering angle $\theta_{Lab} \approx 10^o$ for instance) where DVCS begins to dominate over BH. This allows access to the differential cross section of pure DVCS.

So far, we have considered BH as a sort of "parasite" process to DVCS. However, the argument can actually be turned around. BH is a purely electromagnetic process and as such, is perfectly calculable in QED. The idea is then to take advantage of the BH to study DVCS under a different angle, using the interference of the 2 processes. It has been proposed (see e.g. [4] and references therein) to measure the beam asymmetry (with longitudinally polarized electrons, i.e. the LT' -5th- response function). If there was no BH process, this response function would be 0 (at asymptotically large Q^2 where DVCS is purely transverse and has no longitudinal component at leadig order). However, the interference of the "transverse" DVCS with the longitudinal part of the BH will produce a non-zero signal for this LT' response function. To be explicit, the TL' response function reads :

$$\sigma_{TL'} \propto \frac{1}{2} \sum_{\lambda'_\gamma} \sum_{h'_N} 2Im \left\{ (\mathcal{M}^{+1}(\lambda_{\gamma'}, h'_N; +1/2) - \mathcal{M}^{-1}(\lambda_{\gamma'}, h'_N; +1/2)) \times \mathcal{M}^L(\lambda_{\gamma'}, h'_N; -1/2)^* \right\} \tag{14}$$

Again, the transverse amplitudes ($\mathcal{M}^{\pm 1}$) receive contribution from the DVCS and the BH (exactly calculable) processes whereas the longitudinal amplitude ($\mathcal{M}^L$) comes purely from the BH process (also exactly calculable of course). One should note here that the BH amplitude is purely real whereas the DVCS amplitude has both an imaginary and a real part. Since $\mathcal{R}_{TL'}$ is proportional to an imaginary term, one accesses here the imaginary part of the DVCS amplitude. To illustrate this, we drop the $\frac{1}{x+\xi+i\epsilon}$ and the $E, \tilde{H}$ and $\tilde{E}$ GPD terms in equation 8. Then one roughly measures $H(\xi, \xi, t)$ as $\int_{-1}^{+1} dx \frac{H(x,\xi,t)}{x-\xi+i\epsilon} = \int_{-1}^{+1} dx \frac{H(x,\xi,t)}{x-\xi} - i\pi H(\xi, \xi, t)$. One notes that the GPD information enters here linearly this observable in contrast to differential cross sections, where the GPDs enter quadratically.

This beam asymmetry therefore allows to measure the GPDs at a particular point (i.e. at $x = \xi$) in contrast to the other observable mentioned so far which measure an integral (over x). Clearly, both types of measurements are needed in order to extract the GPDs : the expectation is that, measuring different kinds of integrals (i.e. with different weighting functions) of the GPDs through differential cross sections, beam asymmetry and target asymmetries, we should be able to extract the GPDs. One should also keep in mind that there are already constraints from the various form factors, quark distributions, mesons' distributions amplitues, which appear as integrals over the GDPs. Although it is not possible at this stage to quantify to which accuracy we will actually be able to do this, one should really bear in mind that there is no obstacle in principle in this procedure.

8.2 Modelling GPDs and sensitivities to observables

In this subsection, we discuss some general features of the GPDs and show the sensitivity of the observables mentioned in the previous sections to them. We recall that the GPDs depend upon 3 variables x, ξ and t, of which only -ξ and t- are directly accessible, experimentally.

The simplest parametrization one can think of for the GPD is a "toy" factorized ansatz of the product of a form factor representing the t dependence, with a quark distribution for the x dependence. Such an ansatz straightfowardly satisfies the sum rules and relations with DIS mentionned in section 2. However, it does not take into account any ξ dependence. The ξ dependence can be accounted for with modelling the GPDs through "double distributions" -DDs- [?]. The relation between GPDs and DDs is of the following form :

$$H^q(x,\xi) \quad = \quad \int_{-1}^{1} d\beta \int_{-1+|\beta|}^{1-|\beta|} d\alpha \delta(x-\beta-\alpha\xi) F^q(\alpha,\beta) \tag{15}$$

where the t dependence does not appear here as it is kept factorized in this particular ansatz. F^q is then, up to a known normalization factor, the product of a quark distribution and a meson distribution amplitude. Such an ansatz yields GPDs of the form shown in figure 35 where their x dependence is given for different ξ. We recall that differential cross sections involve the integral over x (weighted by $\frac{1}{x \mp \xi \pm i\epsilon}$) of the GPDs. Such a ξ dependent ansatz will yield different results for such an observable as compared to a ξ independent one. Also, the value of the GPD at $x = \xi$, accessible through the beam asymmetry in DVCS, is a strong contraint for any GPD modelling.

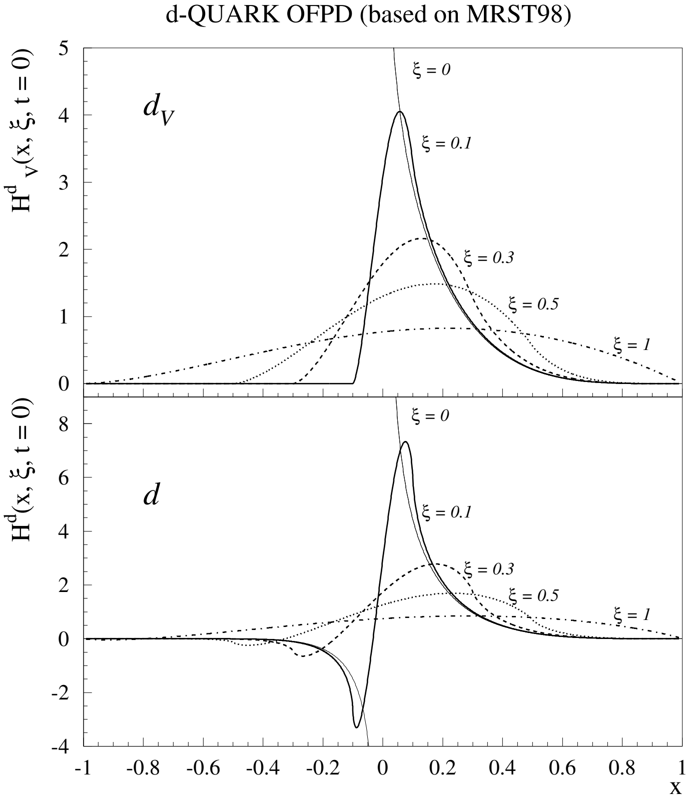

Figure 35: Example of the x dependence of a GPD (H here) at t=0 for different ξ. Upper panel : valence down quark GPD, lower panel : total down quark GPD. The thin lines (ξ=0) correspond to the ordinary d-quark distributions (MRST98 parametrization at Q^2=2 GeV^2).

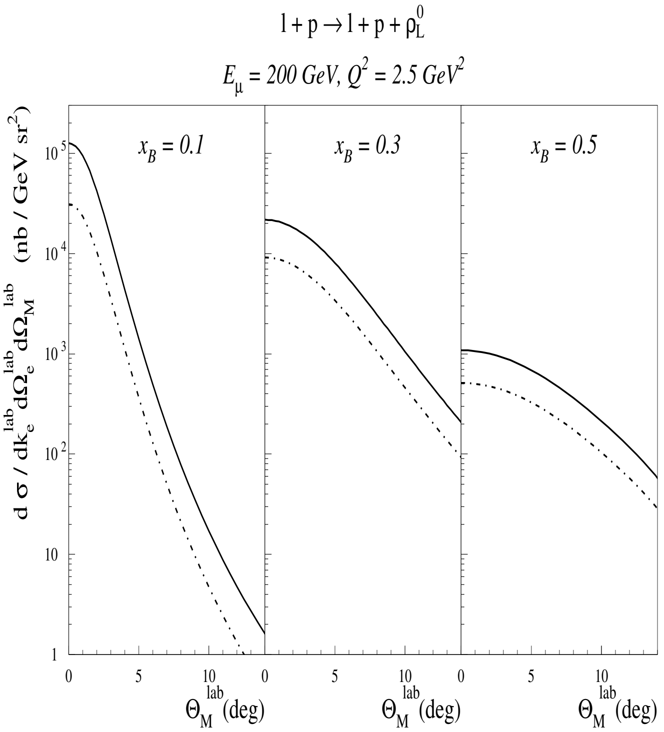

Figure 36: Angular dependence of the leading order amplitudes for ρ^0_L at Q^2=2.5 GeV^2. The prediction with a ξ-dependent ansatz for the GPDs (full lines) is compared with a ξ-independent ansatz for the GPDs (dotted lines).

Figure 36 shows a comparison between a ξ-dependent and a ξ-independent model for the GPD, for the differential cross section of ρ^0_L production. The difference is about a factor 2 and can be distinguished in our proposed experimental program.

Also, the way the quark distributions enter the DDs has to be tested. For example, they could enter with some power [25], i.e. $(q(x))^b$, where the exponent b could be different for valence and sea quarks. Such ansatz still satisfies the relations linking the quark distributions and the GPDs by proper normalization of the DDs. Figures 37 shows the sensitivity of the DVCS beam asymmetry to such sets of b parameters for a typical CEBAF kinematics.

So far, we have assumed that the t dependence of the GPDs was factorizing. Radyushkin et al. have proposed an interplay between the t and x variables yielding a t-dependence for the DDs of the form $\approx e^{-t/x}$. Such form produces a "shrinkage" (somewhat similar to the Regge-type shrinkage, although from a different origin) with increasing energies (decreasing x). Observation of such shrinkage would be a strong constraint for the t dependence of any model.

Finally, we mention the notion of "D-term". So far, we have assumed that the GPDs could be written in terms of DDs. However, it was shown recently (see for instance [26]) that there was another term besides the DDs contributing to the GPDs. This term is called the "D-term" and represents the presence of 2-pions systems in the cloud of the nucleon (it was shown that this term could not be expressed in terms of DDs). It is an extremely important term as such contribution to the structure of the nucleon is completely new information which was never accessed before. This D-term has the following properties :

1. It only contributes to the unpolarized GPDs (H and E).

2. It only contributes to the isoscalar channels (at the quark level, i.e. it only contributes to neutral vector meson production, not to charged vector mesons).

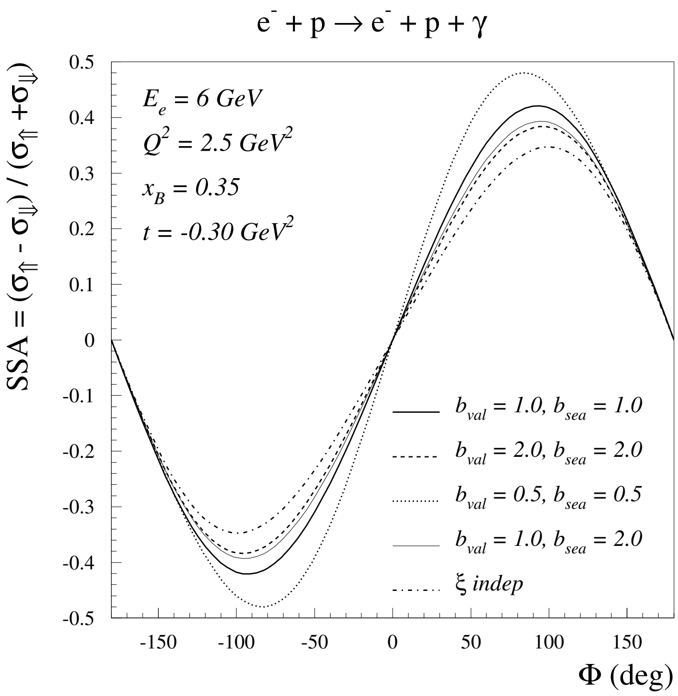

Figure 37: Φ dependence of the beam asymmetry for DVCS for different values of the exponent b of the quark distribution entering the DDs. Also is shown a ξ independent model -i.e., without decomposing the GPDs into DDs.-

3. It only contributes in the region $-\xi < x < \xi$. Figure 38 illustrates, in the framework of a chiral soliton model, how it would change the shape of a GPD (compare to figure 35).

4. It is purely real.

Measurement of this D-term requires measurement of neutral vector meson production or DVCS and at rather large ξ (or x_B). Also, as it is a purely real term, the beam asymmetry of DVCS will not be sensitive to it. We show in figure 39 the sensitivity of the differential cross section of ρ_L^0 production to such D-term for different x_B. As expected, the influence of the D-term manifests itself mostly at large x_B. Such x_B "evolution" needs to be measured for neutral vector mesons and should be absent for pseudo-scalar meson production.

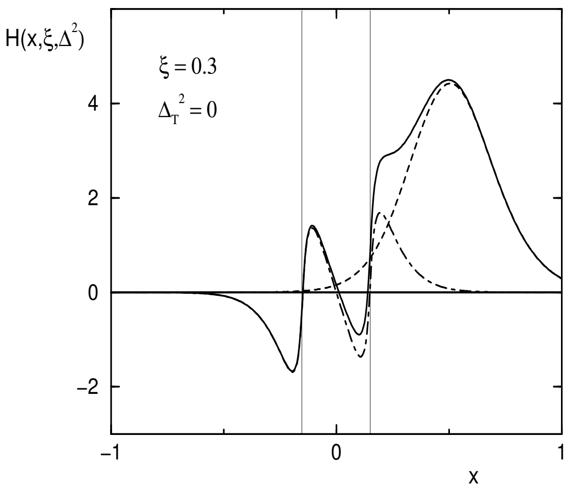

Figure 2: The isosinglet distribution $H(x,\xi,\Delta^2)$ for $\Delta_T^2 = 0$ ($\Delta_T^2 \equiv -\Delta^2 - \xi^2 M_N^2$) and $\xi = 0.3$. *Dashed line*: contribution from the discrete level. *Dashed-dotted line*: contribution from the Dirac continuum according to the interpolation formula, eq. (4.26). *Solid line*: the total distribution (sum of the dashed and dashed-dotted curves). The vertical lines mark the crossover points $x = \pm\xi/2$.

Figure 38: x dependence of the GPD in the framework of Petrov et al. model [26].

18

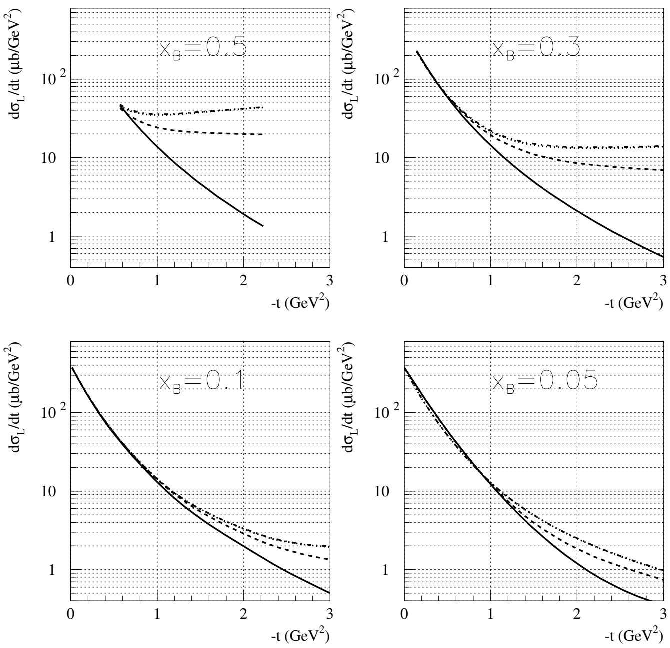

Figure 39: t dependence of the ρ_L^0 differential cross section at different x_B values at Q^2=5 GeV^2 (only the kinematics of the 2 upper plots are accessible with a 11 GeV incident beam). The solid line is the H GPD contribution based only on DDs. The dashed line is the H "DD" contribution with the D-term added. The dashed-dotted line contains the 3 contributions : H "DD" + H D-term + E.

9 Leading order pQCD and power correction for exclusive mechanism

The aim of these section is to summarize where we stand on the (quantitative) comparison between leading order mechanisms and power corrections regarding hard exclusive reactions. We will consider here two main sources of power corrections which we believe are the most important ones, i.e. the intrinsic transverse momentum dependence of partons in the nucleon and the soft "overlap" mechanisms.

The scope of this short document is of course not to present a systematic study of QCD higher twists corrections in exclusive reactions. The aim is just to show that we have all reasons to believe that these corrections can currently be handled and controlled to a reasonnable level.

We will discuss here 2 typical exclusive processes which show asymptotically scaling behavior at large Q2 :

- The π^0, γ, γ^* transition form factor
- The pion form factor

These two cases are at the very basis of our understanding of the situation because experimental data exist and allow quantitative comparison. These 2 form factors (FFs) are really "school cases" and have been studied in detail by numerous groups. They allow to set the stage to extend the techniques to the cases of Deep Virtual Compton Scattering (DVCS) and Deep Virtual Electroproduction of Mesons (DVEM) which are the processes which concern us here most as they give access to the Generalized Parton Distributions (GPDs). For these exclusive electroproduction reactions, there are essentially (except for ρ^0 electroproduction), no experimental data exist to compare to. We therefore need estimates.

The processes can be sorted into two categories (at leading order) :

- Processes involving no gluon exchange (i.e. the π^0, γ, γ^* FF and DVCS),
- Processes involving one gluon exchange (i.e. the pion FF and DVEM).

If we consider as main power corrections the only two sources mentionned in the first paragraph, the essential difference is that processes where no gluon exchange occur are subject only to the transverse momentum dependence corrections whereas for the other type of processes, one has to take also into account soft overlap mechanisms.

9.1 Processes with no gluon exchange - $\pi^0\gamma^*\gamma$ ff and DVCS

The $\pi^0\gamma^*\gamma$ FF has been measured at CORNELL by the CLEO and CELLO experiments up to $Q^2 \approx 10$ GeV^2. The data show a scaling behavior in Q^2 between 5 and 10 GeV^2 (within experimental errors). Leading order pQCD calculations taking an asymptotic distribution amplitude (i.e. $\propto z(1-z)$) for the pion are able to reproduce the normalization of the data in this (asymptotic) scaling region. For $Q^2 < 5$GeV^2, the data show a continuous reduction (of about 30 compared to the leading order result, i.e. we are no more in the scaling regime. This trend of the data can be very well explained with very good numerical agreement down to $Q^2 \approx 1$GeV^2 by the so-called "modified" perturbative approach, i.e. by taking explicitly into account the transverse degrees of freedom of the partons in the nucleon. One takes then for the wave function of the pion a gaussian transverse momentum dependence (i.e. $\exp(k_{perp}/(\sigma * z * (1-z))$. The parameter sigma (related to the average intrinsic transverse momentum of the quarks in the pion) in this ansatz is not a free parameter as it can be deduced from the axial anomaly. The conclusion here is that, basically without any free parameter except for the (gaussian) shape for the transverse momentum distribution of the quarks, one is able to control the deviation to the scaling regime down to 1 GeV^2.

In a very similar fashion, one can apply this "modified" perturbative approach to DVCS (for which no data exist). Similar effects are predicted, i.e. reduction of the cross section by roughly 30% with respect to the leading order regime at $Q^2 \approx 3$GeV^2. This of course has to be compared with data.

9.2 Processes with gluon exchange - F$_\pi$ and DVEM

The pion form factor has been measured at CORNELL (up to Q^2=10 GeV^2) -albeit with quite large error bars. In a similar way to the previous case, it is straightforward to calculate with the "modified" perturbative approach (i.e. taking into account transverse degrees of freedom) the leading order perturbative contribution. It is observed that the asymptotic (scaling) leading order pQCD result is approached only at very large Q^2 (¿30 GeV^{2}2). Similarly to the previous case, the correction including the transverse momentum dependence gives a suppression at lower Q^2. This suppression is however quantitatively much more important in this process (about a factor of 2 around Q^2=5 GeV^2, compared to $20Q^2 \approx 10GeV^2$, the calculation (including the transverse momentum dependence) is about a factor 2 below the data. This indicates a missing contribution. As mentionned before, this other contribution, specific to hard exclusive reactions that proceed through 1-gluon exchange at leading order, is the soft "overlap" mechanism which can compete with the leading order amplitude at intermediate values of Q2. It is indeed observed in calculations that, although the soft overlap contribution drops faster in Q2, one has to go to rather large values of Q^2 before the perturbative 1-gluon exchange contribution dominates. The soft overlap contribution makes up more than half of the total form factor at $Q^2 = 10$ GeV^2 where the sum of the soft overlap and the perturbative one-gluon exchange contribution (corrected for transverse momentum dependence) is compatible with the existing data. This leads to think that other possible competing higher order contributions are not needed and therefore not significant. When comparing to the reported data for the pion electromagnetic form factor, one has to be aware however that these sparse data are rather imprecise at the large Q2 values, as they are obtained indirectly from pion electroproduction experiments through a (model-dependent) extrapolation to the pion pole.

Straightforward extension to the case of hard electroproduction of mesons can be done, in particular for longitudinal ρ^0_L electroproduction for which recent data from HERMES exist (up to $Q^2 = 4GeV^2$) for $5 < W < 10$GeV. In the same fashion as for the pion FF, it is observed that there is substantial reduction of the cross section at the low Q^2 values, before the scaling regime is reached (approximatively a factor 2.5 at Q^2 around 5 GeV^2, which is about the same factor for this correction found by Strikman et al. at higher W where 2-gluon exchanges processes are dominant for vector meson electroproduction). In spite of this important correction common for all 1-gluon exchange processes, it is the same procedure which has been applied for the intrinsic transverse momentum correction in "no-gluon" exchange processes (i.e. $\pi^o\gamma^*\gamma$ FF and DVCS) and absolutely no extra free parameters have been added. We have therefore all reasons to believe that, even though this correction is important, it is consistent through several channels and can be under control. Of course, only cross-comparison with other exclusive reaction channels and other observables (which are currently not existing in the relevant kinematical domain) can confirm this picture.

Another question is, how important the other power correcting mechanism (i.e. the soft overlap for meson electroproduction), which is competing in this lower/intermediate Q^2 region. Estimation of this contribution show that soft overlap contributions do not dominate over the hard amplitude, in fact they are more than a factor of 5 below the hard amplitude including the transverse momentum dependence, as one approaches 10 GeV^2. This behavior is quite different compared with the overlap contribution to F_π. This estimate for the overlap contribution indicates therefore that one is in a more favorable situation with longitudinal meson electroproduction compared to the F_π case. Numerically, the main reason for this is that in the F_π, the gluon in the L.O. diagram is purely spacelike yielding a real quantity whereas in the L.O. meson electroproduction diagram, the exchanged gluon can be both spacelike or timelike according to the value of the quark's momentum fraction x, yielding a complex amplitude. The form factor is therefore comparable to the real part of the hard electroproduction amplitude. As the imaginary part of the hard electroproduction amplitude is numerically by far larger than its real part in the kinematics considered here, the competing (real) soft overlap mechanism might well dominate the real part of the amplitude at the lower Q^2, without dominating the predictions calculated with the total L.O. electroproduction amplitude.

Another argument is that a form factor is intrinsically of a different nature than an electroproduction reaction. In a FF, the process selects 2 active quarks from the valence Fock State of the wave function of the pion which is certainly a small component of the total wave function. Whereas for an electroproduction reaction, the situation is more similar to deep inelastic scattering where the quark which is hit by the virtual photon does not belong to a particular Fock state of the wave function of the nucleon, it is in some sense, integrated over all Fock states.

Our conclusions are :

- It is clear that processes where no gluon exchange occur at leading order suffer less power corrections (due to intrinsic transverse momentum) than processes where 1 gluon exchange occurs (a factor .3 compared to 2 approximatively at some interemediate Q2 in the above examples). For the π^0, γ, γ^* and DVCS, it is estimated that the purely scaling regime occurs around 5-10 GeV2 which should be attainable with JLab@12 GeV.

- Processes where 1 gluon exchange occur at leading order suffer a competing mechanism, the soft overlap process (which drops faster in Q2 than the leading order but which can be dominant at intermediate Q2 values). In particular, it is found that this soft overlap contribution, in the case of the pion FF, is largely dominating the leading order perturbative contribution (power corrected by intrisic transverse momentum dependence) in the accessible Q2 regions at this time. It hass however been found that this soft contribution is NOT dominant for mesons electroproduction reactions. This is due to the very different nature of the 2 processes, although they are both involving 1 gluon exchange.

- Therefore, if we are unable with the current facilities/projects to reach the "true" scaling regime for meson electroproduction, we have reasons to believe that we can control the corrections to be made and therefore have access to and extract the relevant non-perturbative information (i.e. the GPD's) from the data. An evidence for this has been recently given with the realease of the recent HERMES data for the electroproduction of longitudinal ρ^0 around Q^2=4 GeV^2 where a PREDICTION based on a GPD calculation (corrected by intrinsic transverse momentum dependence) matches the experimental data.

- There is as much to learn from the study of the preasymptotic region in particular, when the dominant correcting factor is due to the transverse intrinsic momentum, one can access these transverse quark's distributions.

- Considering that, for the hard meson electroproduction, the corrections related to intrinsic transverse momentum are the most important ones (i.e. the soft overlap contribution being negligeable at some Q2 - 5 GeV2 ??-), and these latter corrections being factorizable (like the correction used by Strikman et al. for 2-gluon exchange processes at high W), ratios such as ρ/ω, $\rho/\phi, \pi^0/\eta$, etc... should then show scaling behavior at relatively low Q^2, perhaps as low as 2 GeV^2.

10 Conclusions

In this program, we are propose a deatiled study of the Generalized Parton Distributions (GPD) via measurements of electroproduction of high energy photons, vector-, and pseudoscalar mesons, above the resonance region, and at large Q^2. An electron beam of 11 GeV energy, and use of an upgraded CLAS detector is assumed.

We have performed simulations and sensitivity studies to a variety of reactions, such as $ep \to e'\rho p$, $ep \to e'\pi^+ n$ and $ep \to e'p\gamma$. For the meson channels, the extraction of the longitudinal part of the cross section is needed. For vector mesons, it will be carried out by studying the angular distribution of the decay pions and for pseudo-scalar mesons, through the Rosenbluth technique. The longitudinal part of these processes is directly comparable to leading order pQCD calculations and predictions in terms of normalization, Q^2, x_B and t dependences [9, 8], ratios, asymmetries, etc....

Among all facilities, at this time, only JLab at 12 GeV can carry out such a general "exclusive" program, in particular Rosenbluth-type L/T separations which is necessary in the pseudo-scalar sector at least in the initial stage until σ_L dominance is established.

This program involves a simultaneous scan of various variables (x_B, Q^2, t), which can be best done using a large acceptance detector such as CLAS. Some part of the program could also be done with specialized equipment employing equipment from other Halls.

We estimate that a broad program can be carried out with an upgraded CLAS on a time scale of a year of beam time.

References

[1] X. Ji, Phys. Rev. Lett. **78**, 610 (1997); Phys. Rev. D **55**, 7114 (1997).

[2] A.V. Radyushkin, Phys. Lett. B **380**, 417 (1996); Phys. Rev. D **56**, 5524 (1997).

[3] M. Guidal, C. Marchand, E. Smith *et al.*, JLab Experiment E99-105.

[4] Y. Roblin, F. Sabatie *et al.*, Experiment proposed at PAC18.

[5] J.C. Collins, L. Frankfurt, and M. Strikman, Phys. Rev. D **56**, 2982 (1997).

[6] M. Vanderhaeghen, P.A.M. Guichon, and M. Guidal, Phys. Rev. Lett. **80**, 5064 (1998).

[7] P.A.M. Guichon and M. Vanderhaeghen, Prog. Part. Nucl. Phys., Vol. 41, 125 (1998).

[8] M. Vanderhaeghen, P.A.M. Guichon, and M. Guidal, Phys. Rev. D **60**, 094017 (1999).

[9] L. Mankiewicz, G. Piller, and A. Radyushkin, Eur. Phys. J. C **10**, 307, (1999).

[10] L. Frankfurt, P. Pobylitsa, M. Poliakov, and M. Strikman, Phys. Rev. D **60** 014010, (1999).

[11] M. Arneodo et al., Nucl.Phys. **B429** (1994) 503.

[12] M.R. Adams et al., Z.Phys.C **74** (1997) 237.

[13] M. Derrick et al., Phys.Lett.B **356** (1995) 601.

[14] S.J. Brodsky et al., Phys.Rev.D **50** (1994) 3134.

[15] L. Frankfurt, W. Koepf and M. Strikman, Phys.Rev.D **54** (1996) 3194.

[16] J.A. Crittenden (for ZEUS Collaboration), presented at Photon'97, May 1997.

[17] A. Airapetian et al., HERMES Collaboration, submitted to Eur.Phys.J., hep-ex/000402

[18] P. Joos et al., Nucl.Phys. **B113** (1976) 53.

[19] D.G.Cassel et al., Phys.Rev.D **24** (1981) 2787.

[20] C.J. Bebek et al., Phys. Rev. D **13**, 1693 (1978).

[21] E.S. Smith, "Fast Monte Carlo Program for the CLAS Detector", CLAS-Note 90-003, (1990).

[22] M. Morlet and J. Van de Wiele, private communication.

[23] J. J. Sakurai, Phys.Rev.Lett **22** (1969) 981.

[24] R. Jakob, P. Kroll and M. Raulfs, J.Phys.G **22**, 45 (1996); P. Kroll and M. Raulfs, Phys.Lett.B **387**, 848 (1996).

[25] M. Vanderhaeghen, private communication.

[26] V. Yu. Petrov, P.V. Pobylitsa, M.V. Polyakov, I. Bornig, K. Goeke and C. Weiss, Phys. Rev. D **57** 4325, (1998).

[27] M. Guidal and M. Vanderhaeghen, "Computer Code for DVCS and BH Calculations", Private communications.

[28] Upgrading CLAS to Higher Energy